



**HAL**  
open science

## Halogen bond in separation science: A critical analysis across experimental and theoretical results

Paola Peluso, Victor Mamane, Alessandro Dessì, Roberto Dallochio,  
Emmanuel Aubert, Carlo Gatti, Debby Mangelings, Sergio Cossu

### ► To cite this version:

Paola Peluso, Victor Mamane, Alessandro Dessì, Roberto Dallochio, Emmanuel Aubert, et al.. Halogen bond in separation science: A critical analysis across experimental and theoretical results. *Journal of Chromatography A*, 2020, 1616, pp.460788. 10.1016/j.chroma.2019.460788 . hal-02445333

**HAL Id: hal-02445333**

**<https://hal.science/hal-02445333>**

Submitted on 26 May 2020

**HAL** is a multi-disciplinary open access archive for the deposit and dissemination of scientific research documents, whether they are published or not. The documents may come from teaching and research institutions in France or abroad, or from public or private research centers.

L'archive ouverte pluridisciplinaire **HAL**, est destinée au dépôt et à la diffusion de documents scientifiques de niveau recherche, publiés ou non, émanant des établissements d'enseignement et de recherche français ou étrangers, des laboratoires publics ou privés.

2 **Halogen bond in separation science:**

3 **a critical analysis across experimental and theoretical results**

4 Paola Peluso,<sup>a,\*</sup> Victor Mamane,<sup>b,\*</sup> Alessandro Dessì,<sup>a</sup> Roberto Dallocchio,<sup>a</sup> Emmanuel Aubert,<sup>c</sup>  
5 Carlo Gatti,<sup>d</sup> Debby Mangelings,<sup>e</sup> and Sergio Cossu<sup>f</sup>

6 <sup>a</sup> Istituto di Chimica Biomolecolare ICB, CNR, Sede secondaria di Sassari, Traversa La Crucca 3, Regione Balduca,  
7 I-07100 Li Punti - Sassari, Italy

8 <sup>b</sup> Institut de Chimie de Strasbourg, UMR CNRS 7177, Equipe LASYROC, 1 rue Blaise Pascal, 67008 Strasbourg Cedex,  
9 France

10 <sup>c</sup> Cristallographie, Résonance Magnétique et Modélisations (CRM2), UMR CNRS 7036, Université de Lorraine, Bd des  
11 Aiguillettes, 54506 Vandoeuvre-les-Nancy, France

12 <sup>d</sup> CNR-ISTM, Istituto di Scienze e Tecnologie Molecolari, via C. Golgi 19, 20133 Milano, Italy

13 <sup>e</sup> Department of Analytical Chemistry and Pharmaceutical Technology (FABI), Center for Pharmaceutical Research  
14 (CePhaR), Vrije Universiteit Brussel – VUB, Laarbeeklaan 103, B-1090 Brussels, Belgium

15 <sup>f</sup> Dipartimento di Scienze Molecolari e Nanosistemi DSMN, Università Ca' Foscari Venezia, Via Torino 155,  
16 I-30172 Mestre Venezia, Italy

17  
18 \* Corresponding authors. E-mail address: paola.peluso@cnr.it. Tel.: +39 079 2841218. E-mail address: vmamane@unistra.fr.  
19 Tel.: +33 368 851612.

20 **ABSTRACT**

21 The halogen bond (XB) is a noncovalent interaction involving a halogen acting as electrophile and a  
22 Lewis base. In the last decades XB has found practical application in several fields. Nevertheless,  
23 despite the pivotal role of noncovalent interactions in separation science, investigations of XB in this  
24 field are still in their infancy, and so far a limited number of studies focusing on solid phase extraction,  
25 liquid-liquid microextraction, liquid-phase chromatography, and gas chromatography separation have  
26 been published. In addition, in the last few years, our groups have been systematically studying the  
27 potentiality of XB for HPLC enantioseparations. On this basis, in the present paper up-to-date results  
28 emerging from focused experiments and theoretical analyses performed by our laboratories are

29 integrated with a descriptive presentation of XB features and the few studies published until now in  
30 separation science, with the aims to provide a comprehensive and critical discussion of the topic, and  
31 account for some still open issues in this field.

32

33 *Keywords:* Chromatography, Enantioseparation, Halogen bond, Molecular modelling, Separation  
34 science

35

36

## 37 **1. Introduction**

38 Separation science deals with theory, methods and technologies related to separation of chemical  
39 compound mixtures [1-3]. A separation process must be able to discriminate molecules in a  
40 multicomponent mixture. Therefore, the knowledge of size, shape, and structure of the molecular  
41 components of a mixture is a basic requirement to design a tailored separation system. Indeed, properties  
42 of the molecules which are involved in the separation process determine separation mechanisms and  
43 noncovalent interactions which underlie mixture formation and separation.

44 When molecules are at work to carry out a specific function in molecular and supramolecular  
45 systems, they relate to each other by means of noncovalent interactions [4,5], which represent the  
46 essential elements of the code by which molecules are able to transfer the information contained in their  
47 structure [6]. These molecular relationships underlie mechanisms in several fields [7], and also  
48 make noncovalent interactions a modern tool for design, preparation and function of advanced processes  
49 and materials in separation science [8].

50 Among noncovalent interactions, in the last decades halogen bonds (XBs) have found practical  
51 applications in several fields covering catalysis, crystal engineering, functional and soft materials,  
52 molecular recognition, supramolecular chemistry and biological, medicinal and pharmaceutical  
53 chemistry [9-11]. Nevertheless, separation processes promoted by XB are reported in smaller degree  
54 [8,12-16]. In particular, despite the pivotal role of noncovalent interactions in LC enantiomer distinction  
55 [17,18], surprisingly, for a long time XBs were unexplored in the enantioseparation science [19].

56 Various reasons have contributed to make the study of XB in separation science challenging. First,  
57 halogen substituents can contribute to separation and molecular recognition process by playing multiple  
58 roles (hydrophobic site, electron-withdrawing atom, repulsive interaction site, HB acceptor), and the  
59 presence of electrophilic regions on bound halogens has to be confirmed theoretically. Indeed, XB  
60 comprehension mostly depends on its physical description at theoretical level [20-22]. Then, often  
61 separation processes occur in solution, and the study of XB in solution [23] is a more demanding task

62 compared to solid state studies. For example, the chromatography environment is a complex solvated  
63 system. Finally, limited availability of brominated and iodinated analytes makes the study of halogen  
64 effect on separation processes challenging.

65 In this perspective, the aim of this paper is to provide a critical analysis of the topic. For this purpose,  
66 firstly, XB is profiled by describing its main features. Secondly, the few studies on XB applications in  
67 separation science reported so far in the literature are discussed. Then, with the aim to explore and  
68 clarify some still open issues, we described herein up-to-date results performed by our laboratories  
69 specifically for this purpose and emerging from i) a theoretical re-examination of some literature studies  
70 using the density functional theory (DFT) method, and ii) an experimental exploration under  
71 supercritical fluid chromatography (SFC) conditions. This multidisciplinary approach is in agreement  
72 with recent trends in separation science where theoretical methods are integrating more and more with  
73 experiments in order to develop separation systems with high capacity, robustness, and selectivity.

## 74 **2. Experimental**

### 75 *2.1 Chemicals*

76 Compounds **39i**, **39s**, and **39v** were synthesized as reported [24]. Pure enantiomers of compounds **39i**,  
77 **39s**, and **39v** were obtained by HPLC enantioseparation and their absolute configuration were assigned  
78 on the basis of X-ray diffraction or by comparison of theoretical/experimental electronic circular  
79 dichroism spectra, as previously described [25].

### 80 *2.2 Chromatography*

81 For analyses under normal phase (NP) elution conditions, a Merck-Hitachi Lachrom Elite gradient  
82 HPLC system with photodiode array detection (Tokyo, Japan) and an Agilent Technologies (Waldbronn,  
83 Germany) 1100 Series HPLC system (Agilent Technologies ChemStation Version B.04.03  
84 chromatographic data software) were employed. Analyses under SFC were performed by using a Waters  
85 UPC<sup>2</sup> SFC system with photodiode array detection. The carbon dioxide (CO<sub>2</sub>) advised by the  
86 manufacturer of the SFC equipment was used, i.e. quality 2.7 (purity >99.7%) (Linde Gas, Grimbergen,

87 Belgium). Lux Cellulose-1 (Phenomenex, USA) (cellulose *tris*-3,5-dimethylphenylcarbamate; 5  $\mu\text{m}$ ),  
88 was used as a chiral column (250  $\times$  4.6 mm). HPLC grade *n*-hexane, and 2-propanol were purchased  
89 from Sigma-Aldrich (Taufkirchen, Germany). Analyses were performed in isocratic mode at 25°C. The  
90 flow rate was set at 0.8 and 1 ml/min. The enantiomer elution order (EEO) was determined for  
91 compounds **39i**, **39s**, and **39v** by injecting enantiomers of known absolute configuration.

### 92 2.3 Computational

93 Geometry optimization and computation of electrostatic potentials mapped on 0.002 au isosurfaces  
94 ( $V_S(\mathbf{r})$ ) and related parameters ( $V_S(\mathbf{r})$  extrema, maxima ( $V_{S,\text{max}}$ ) and minima ( $V_{S,\text{min}}$ ) values, given in  
95 kJ/mol or au) were performed and graphically generated by using Spartan' 10 Version 1.1.0  
96 (Wavefunction Inc., Irvine, CA) [26] (DFT method with the B3LYP functional and the 6-311G\* basis  
97 set) and Gaussian 09 (Wallingford, CT 06492, USA) [27] (DFT/B3LYP/def2-QZVP and DFT/M06-  
98 2X/def2-QZVP). Values of  $V_S(\mathbf{r})$  were used as an indicator of the molecular charge distribution [28]. On  
99 the isosurface, colours towards red depict negative mapped potentials, while colours towards blue depict  
100 positive potentials and colours in between (orange, yellow, green) depict intermediate values of the  
101 mapped potential. Search for the exact location of  $V_{S,\text{max}}$  and  $V_{S,\text{min}}$  was made through the Multiwfn code  
102 [29] and through its module enabling quantitative analyses of molecular surfaces [30] for several  
103 isovalue surface fields and mapped properties thereon. For compounds **39s**, **39t**, and **39u**, electrostatic  
104 potential source function decomposition analysis was performed as reported [31].

## 105 3. Halogen bond

### 106 3.1. Brief history

107 The first observed XB-based association was the iodine-ammonia complex ( $\text{I}_2 \cdots \text{NH}_3$ ) obtained by  
108 Colin in 1814 through the reaction of iodine and gaseous ammonia [32]. Later the same complex was  
109 reported by Guthrie upon reaction between iodine and liquid ammonia [33]. Then, other theoretical and  
110 experimental studies were performed, nevertheless for a long time these data were unable to provide a  
111 comprehensive picture of the XB [9].

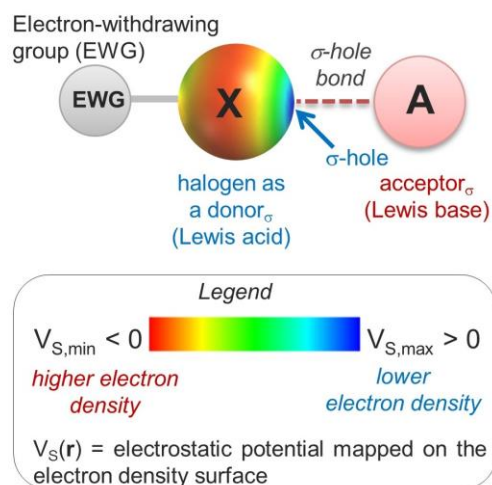
112 On the contrary, in the late twentieth century, important observations and experiments brought the  
113 great potential of XB to light, and allowed to recognize that the electrophilic behaviour of halogens is a  
114 commonplace event rather than exceptional, occurring in the solid, liquid and gas phase [9,10]. The first  
115 use of the term XB can be traced back to the study of Zingaro and Hedges in 1961 [34], the authors  
116 describing the complexes formed between halogens and phosphine oxides or phosphine sulphides. In  
117 1968, Bent published a review on the chemistry of donor-acceptor adducts, where he treated about  
118 “*Organic Molecules with Oxygen Atoms as Electron Donors and Halogen Atoms as Acceptors*” and  
119 “*Molecules with Halogen Atoms as Electron Donors and/or Acceptors*”. In this paper, the author  
120 highlighted the distinctive geometric features of the interactions, evidencing that the distances between  
121 the electron donor atom and the halogen atom were shorter than the sum of their respective van der  
122 Waals radii [35]. Later, in his Nobel lecture, Hassel considered that “*Particular importance may be*  
123 *attributed to complexes in which direct bonding exists between one atom belonging to the donor*  
124 *molecule and another atom belonging to the acceptor molecule. Complexes of this kind are above all*  
125 *those formed by donor molecules containing atoms possessing "lone pair electrons" and halogen or*  
126 *halide molecules*” [36].

127 Finally, in 2013 the International Union of Pure and Applied Chemistry issued the “Definition of the  
128 halogen bond (IUPAC recommendations 2013)” stating that “*a halogen bond occurs when there is*  
129 *evidence of a net attractive interaction between an electrophilic region associated with a halogen atom*  
130 *in a molecular entity and a nucleophilic region in another, or the same, molecular entity*” [37].

### 131 3.2. Halogen bond and $\sigma$ -hole bonds

132 In 1992, Brinck, Murray and Politzer proposed the first theoretical explanation of the XB introducing  
133 two basic concepts: the anisotropic charge distribution on bound halogens and the definition of the  $\sigma$ -  
134 hole as a region of electronic charge density depletion, which is located on the surface of halogen atoms  
135 and usually characterized by a positive electrostatic potential [38]. On this basis, the XB originates from

136 the anisotropic charge distribution which characterizes bound halogens, in particular when they are  
 137 bound to electron withdrawing groups (EWGs). It means that an area of lower electron density, located  
 138 on the elongation of the covalent bond, the  $\sigma$ -hole, coexists with an area of higher electron density,  
 139 which forms a belt orthogonal to the covalent bond (Fig. 1) [39].



140

141 **Fig. 1.** General description of  $\sigma$ -hole and halogen bond.

142 Other atoms were found to interact by means of  $\sigma$ -hole regions, therefore XBs are a subset of the so-  
 143 called  $\sigma$ -hole bonds. This wide family of noncovalent interactions involves an electrophilic region of  
 144 electronic charge density depletion (the  $\sigma$ -hole) centred on bound atoms of groups 13-18 ( $\sigma$ -hole  
 145 donors), which behave as Lewis acids, and a  $\sigma$ -hole acceptor, a Lewis base (Table 1) [40].

146

**Table 1**

147

Noncovalent interactions based on electrophilic  $\sigma$ -holes.

148

$\sigma$ -hole bond		
$\sigma$ -hole donor (Lewis acid)	-----	$\sigma$ -hole acceptor (Lewis base)
Donor $_{\sigma}$ (Lewis acid)	$\sigma$ -hole bond	Acceptor $_{\sigma}$ (Lewis base)
B, Al, Ga, In, Tl (group 13)	Triel bond	
C, Si, Ge, Sn (group 14)	Tetrel bond	
P, As, Sb, Bi (group 15)	Pnictogen bond	O, N, S, halogen,
S, Se, Te (group 16)	Chalcogen bond	$\pi$ -donor, anion
F, Cl, Br, I (group 17)	Halogen bond	
Kr, Xe (group 18)	Aerogen bond	

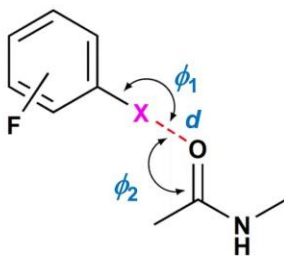
149

150

151 3.3. Features of the halogen bond

152 The anisotropic charge distribution explains the amphoteric behaviour of the halogens which behave  
153 as Lewis bases, or as XB donors with properties of Lewis acids able to interact with an acceptor through  
154 the  $\sigma$ -hole. The most important feature of the XBs is tunability, the strength of a XB depending on the  
155 properties of donor, acceptor and medium, and it increases as the polarizability and the electronegativity  
156 of the halogen increases and decreases, respectively. So, XB strength increases following the order  $F <$   
157  $Cl < Br < I$ , bromine and iodine being considered as more powerful XB donors. Concerning medium, in  
158 general solvents possessing hydrogen bond donor functionalities destabilize the XBs because of XB-  
159 hydrogen bond competition. Indeed, molecules with properties as Lewis bases can act as acceptors  
160 towards both halogen and hydrogen bond donors.

161 Another distinctive feature of the XB is directionality (Fig. 2), with defined geometrical parameters,  
162 angles and distance (typical values for  $I \cdots O$  contacts:  $2.8 \text{ \AA} \leq d_{I \cdots O} \leq 3.4 \text{ \AA}$ , sum of I,O vdW radii being  
163  $3.5 \text{ \AA}$  [41]). In this regard, a parameter to measure the strength of the XB is the penetration parameter  
164 (*p.p.*) [24] which is calculated as the percentual reduction of the sum of van der Waals radii of the  
165 interacting atoms, indicating the penetration degree of the van der Waals spheres.



GEOMETRICAL PARAMETERS

$\phi_1$  C—X—O angle (reference value  $180^\circ$ )

$\phi_2$  X—O=C angle (reference value  $120^\circ$ )

$d_{X \cdots O}$  (Å) typical distances 80-98% sum of van der Waals radii

PENETRATION PARAMETER % =

$$100 \times \left\{ \left( \frac{d_{X \cdots A}}{r_{vdW} X + r_{vdW} A} \right) - 1 \right\}$$

where X = halogen, A = acceptor,  
 $d_{X \cdots A}$  = interatomic distance,  
and  $r_{vdW}$  is the van der Waals radius

166

167 **Fig. 2.** Geometrical parameters of the halogen bond.

168 Due to the physical nature of the XBs, computational tools and studies *in silico* have greatly  
169 contributed to their understanding [20], explaining experimental results and guiding experiment design.  
170 In particular,  $\sigma$ -hole being a region of electronic charge density depletion, calculated  $V_S(\mathbf{r})$  has been  
171 widely used as an indicator of the anisotropy of the molecular charge distribution. In this regard, the  
172 evaluation of the  $V_{S,\max}$  on the halogen surfaces allows for a quantitative estimation of the  $\sigma$ -hole depth  
173 [42] which, in turn, determines the capability of a halogen as XB donor.

174 Nowadays the nature of XBs still remains matter of hot discussion in order to define the relative  
175 importance of electrostatic, dispersion, charge transfer and polarization contributions when XB occurs  
176 [9,43,44]. In this regard, it is worth noting that the studies on the nature of the XB, which have been  
177 published so far, tend to be often contradictory in their conclusions. It is likely that this apparent lack of  
178 coherence is due to the fact that the relative importance of the different contributions depends on the  
179 system, which consists of donor, acceptor and medium [10].

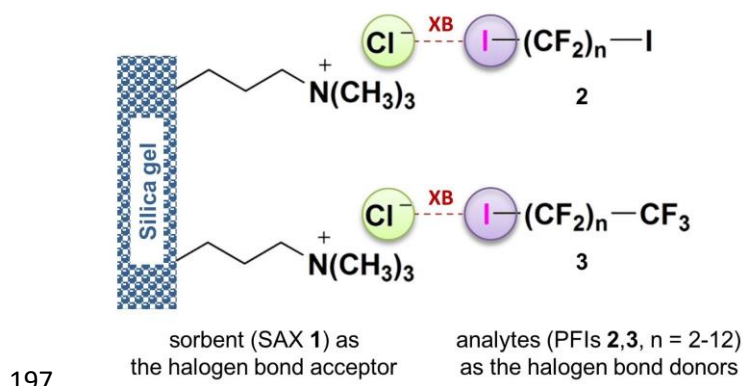
180 On the other hand, the general features of the XB are well explained on the basis of its electrostatic  
181 nature. In particular, a pure electrostatic model gives reasonable correlations to experimental data  
182 gathered in apolar solvents, even if it is unsuitable for the description of XBs in polar systems [23].

183 Recently, Clark proposes a protocol consisting of three level of interaction for the analysis of weak  
184 intermolecular interactions such as XB: i) a first level containing the classical  $\delta^+ - \delta^-$  electrostatic  
185 interactions (*permanent electrostatic interactions*) that can be evidenced by inspecting the unperturbed  
186  $V_S(\mathbf{r})$  at the standard isodensity surfaces of an isolated molecule [28], ii) the second level improves the  
187 previous view by introducing the mutual polarisation of interacting molecules (*induced electrostatic*  
188 *interactions*), and iii) finally, the third level includes dispersion, which is not is not a real, measurable  
189 quantity and can only be observed as a difference between mean-field calculations and those that  
190 consider electron correlation [45].

#### 191 **4. Halogen bond in separation science: a literature survey**

192 4.1. Solid-phase extraction of iodoperfluoroalkanes

193 In 2012, Jin and co-workers described the unprecedented utilization of XB in the solid phase  
194 extraction of perfluorinated iodoalkanes (PFIs) from *n*-hexane. A strong anion-exchange (SAX) sorbent  
195 (1) (Fig. 3) functioning as XB acceptor was used, which forms an associate with PFIs 2 and 3 behaving  
196 as XB donors [12].



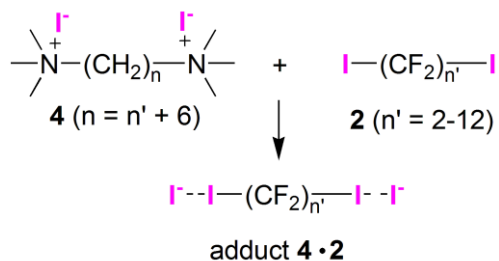
198 **Fig. 3.** Interaction models of the PFIs (2,3) and Cl<sup>-</sup> on the SAX sorbent (1).

199 PFIs are persistent organic pollutants, being key intermediates for the synthesis of fluorochemicals  
200 and fluoropolymers. In this study, following a multidisciplinary approach, nine PFIs, as test probes, were  
201 analysed by UV, <sup>19</sup>F NMR and Raman spectroscopies in order to demonstrate the occurrence of C-  
202 I...Cl<sup>-</sup> XB interactions. The results showed that the adsorptivities of SAX for the α,ω-  
203 diiodoperfluoroalkanes (DIPFAs) 2 were stronger than those for the monoiodo-PFIs 3. In particular,  
204 SAX proved to have no adsorption for hexafluorobenzene, which has no properties as XB donor.

205 Therefore, the application of XB in solid-phase extraction provides a new retention mechanism in  
206 extraction processes. Moreover, this investigation paved the way to the utilization of XB in  
207 chromatography and to the idea, which our group will develop later (§ 5), that XBs could also work on  
208 chiral sorbents to promote enantiomer distinction.

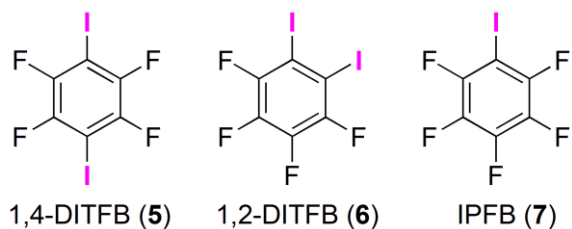
209 It is worth mentioning that in 2009 Resnati and co-workers had showed that the organic salts  
210 bis(trimethylammonium)alkane diiodides 4 (Fig. 4) could resolve mixtures of DIPFAs 2 by means of  
211 crystallization from solution [46] promoted by I...I XB interactions. Interestingly, the solid-state salts

212 could also selectively bind the DIPFAs from the vapor phase, yielding the same adducts formed from  
 213 solution.



214  
 215 **Fig. 4.** XB adduct between bis(trimethylammonium)alkane diiodides (**4**) and DIPFAs (**2**).

216 Later, the group of Jin also investigated the adsorption of iodoperfluoroarenes (IPFARs) (Fig. 5) on  
 217 SAX promoted by XB, using again *n*-hexane as a solvent [47].

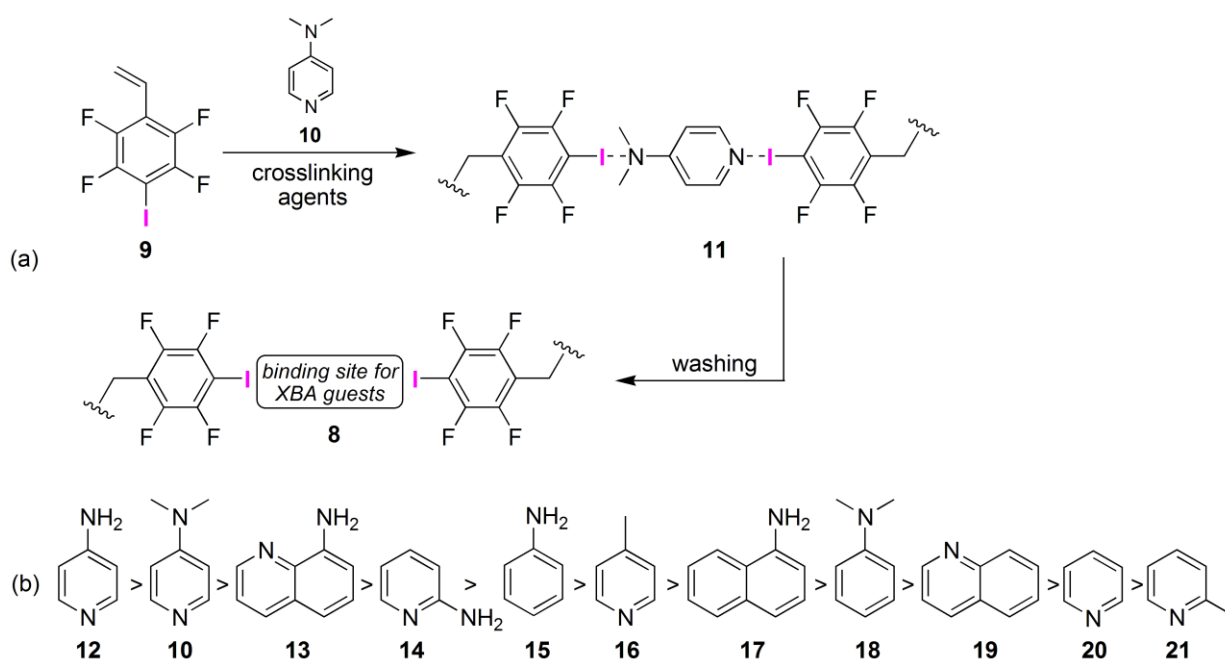


219 **Fig. 5.** Structures of IPFB, 1,2- and 1,4-DITFB.

220 On the basis of  $^{19}\text{F}$  NMR titration experiments, UV spectrometric titrations and theoretical  
 221 calculations, the authors showed that  $\text{Cl}^-$ , as the XB acceptor, is better than  $\text{Br}^-$  and  $\text{I}^-$ . The adsorption  
 222 efficiency of IPFARs on SAX followed the order 1,4-DITFB (**5**)  $\approx$  1,2-DITFB (**6**) > IPFB (**7**), with no  
 223 significant adsorption of bromoperfluoroarenes. Interestingly, prominent red shifts of characteristic  
 224 Raman spectra showed that XB is unambiguously the main driving force of the adsorption process.

#### 225 4.2. Molecularly imprinted polymers

226 In 2005, a molecularly imprinted polymer (**8**) (Fig. 6) bearing XB-based binding sites was developed  
 227 by Takeuchi and co-workers for application in separation science [16]. The formation of this imprinted  
 228 polymer host was obtained by the polymerization of the functional monomer 2,3,5,6-tetrafluoro-4-  
 229 iodostyrene (**9**), as the XBdonor, with divinylbenzene and styrene as cross-linking agents, in the  
 230 presence of 4-(dimethylamino)pyridine (**10**) as the XB acceptor templating guest.



231

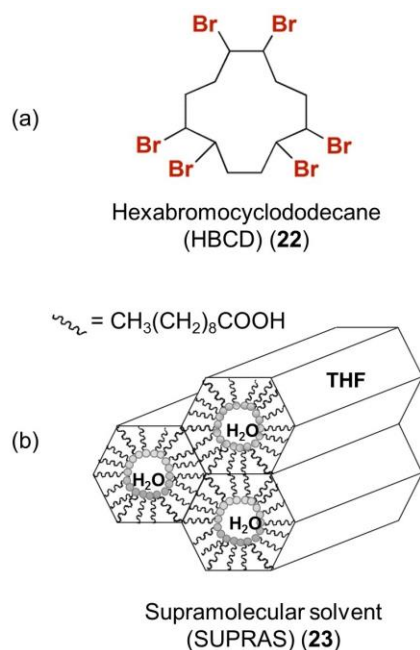
232 **Fig. 6.** (a) Preparation scheme of the molecularly imprinted polymer developed using 4-(dimethylamino)pyridine as XB  
 233 acceptor template; (b) affinity order of the XB acceptor guests.

234 Indeed, the authors had envisaged that the XB acceptor template could recognize the XB donor sites  
 235 on the host polymer, imprinting the molecular shape of the guest into the polymer (11) and generating  
 236 specific binding sites selective for 10 and its structural analogues. On this basis, the binding affinity of  
 237 the imprinted polymer was investigated by using XB acceptors 10 and 12-21 bearing either aliphatic or  
 238 aromatic nitrogen groups. As expected, the 4-aminopyridine guests 12 and 10 showed the highest  
 239 affinities for the porous polymer, which exhibited a high affinity for the less bulky 4-aminopyridine  
 240 (12), suggesting that nitrogen basicity and steric hindrance may influence the recognition mechanism.

#### 241 4.3. Halogen bond in liquid-liquid microextraction

242 Recently, Sicilia and co-workers proposed a solubilisation mechanism based on XB and dispersion  
 243 interactions for increasing the efficiency in the liquid-liquid microextraction of  
 244 hexabromocyclododecane (HBCD) stereoisomers (22) (Fig. 7) in river water, by using a supramolecular  
 245 solvent (SUPRAS) (23), which is made up of inverted hexagonal aggregates of decanoic acid in  
 246 tetrahydrofuran and water [13,48]. HBCDs are brominated flame retardants used in industry that can be  
 247 released into the environment. For SUPRAS 23, two types of interactions with 22 were hypothesized:

248 XB through the oxygen atom of the carboxylic acid and dispersion interactions in the hydrocarbon  
249 chains.



250  
251 **Fig. 7.** (a) Structure of HBCD; (b) scheme of the nanostructure of SUPRAS.

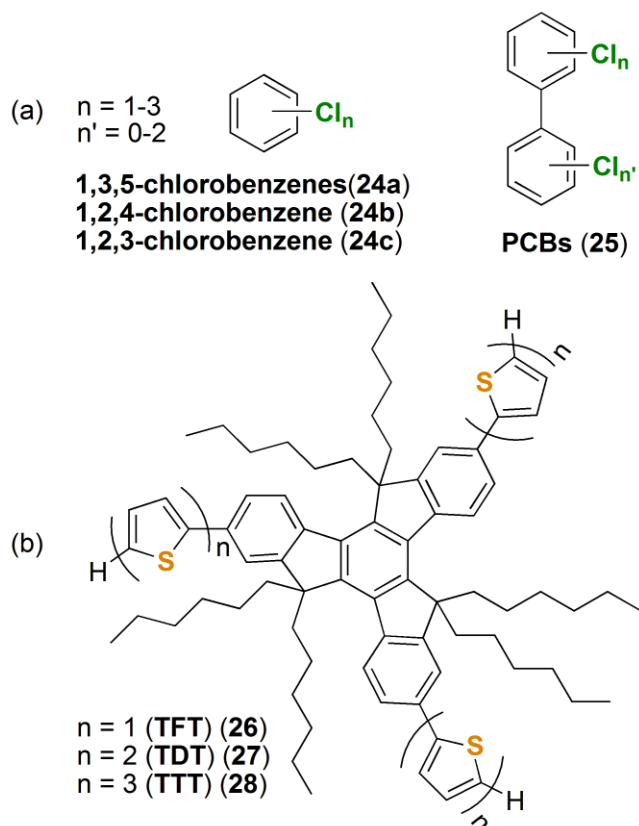
252 The same XB-based microextraction procedure had been previously proposed by the same group for  
253 speeding up the extraction of HBCD in soils and sediments [49] and fish [50]. Unfortunately, these  
254 studies suffer from the fact that the proposed mechanism was not supported by spectroscopic analyses or  
255 theoretical calculations on both donor (HBCD) and acceptor (SUPRAS).

#### 256 4.4. Halogen bond in gas-chromatography separation of haloarenes

257 The utilization of XB can open new possibilities for GC separation of halocarbons, a class of  
258 industrially relevant compounds. In particular, chlorobenzenes **24** and polychlorobiphenyls (PCBs) **25**  
259 (Fig. 8a) are key molecules for chemical industries and environmental analysis.

260 In the last few years, Qi, Wang and co-workers developed thiophene-functionalized truxene  
261 derivatives (TFT **26**, TDT **27**, TTT **28**) [14,51] as new types of stationary phases for GC separations  
262 (Fig. 8b). The separation ability of these supports towards **24** and **25** was explored. A longer retention  
263 was observed for **24c**, which was attributed by the authors to a strong XB between the chlorines of the

264 analyte (XB donors) and the sulfur atoms (XB acceptors) of the **26** side chains. Moreover, hypothesizing  
265 again a XB-based retention mechanisms, the authors performed the separation of three trichlorobenzene  
266 isomers on **28** with the retention order **24a** < **24b** < **24c**.



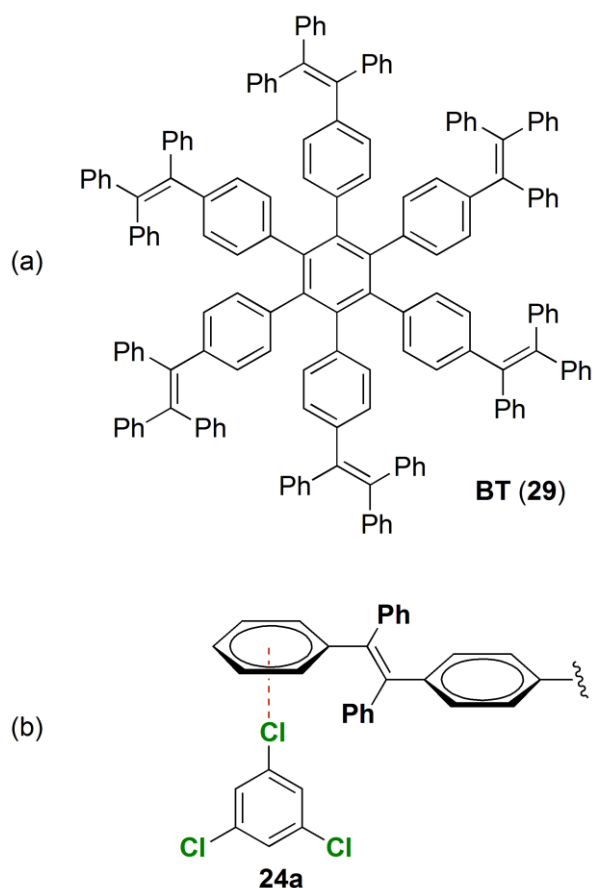
267

268 **Fig. 8.** (a) analytes separated on truxene-based stationary phases; (b) Chemical structure of TFT, TDT and TTT.

269 Later, the same group reported the development of a propeller-like hexaphenylbenzene-based  
270 hydrocarbon material (BT) (**29**) (Fig. 9a) [52] which was used as the stationary phase for capillary GC.  
271 The BT capillary column showed weak polarity and interesting selectivity for aromatic compounds, the  
272 stationary phase being characterized by  $\pi$ -electron toroidal delocalization and intrinsic microporosity. In  
273 particular, the trichlorobenzene isomers were well resolved, the authors hypothesizing combined  
274 interactions of XB ( $\text{Cl}\cdots\pi$ ) (Fig. 9b),  $\pi$ - $\pi$  stacking and van der Waals.

275 Very recently, Qi, Huang and co-workers published a series of papers dealing with the development  
276 of triptycene (TP)-based materials **30-33** for capillary GC separations (Fig.10) [15,53,54]. These  
277 stationary phases exhibited high-resolution performances for a wide range of analytes, especially

278 halogenated structural and positional isomers. In particular, the fact that the stationary phase **30** retained  
279 bromohexane longer than cyclohexanone was explained by means of a XB involving the bromine  
280 substituent of the analyte. The same explanation was used to justify the elution sequence nitrobenzene  
281 (**34**) < 1,3,5-trichlorobenzene (**24a**) and naphthalene (**35**) < *m*-dibromobenzene (**36**), which appeared to  
282 be against the order of boiling points of the analytes.

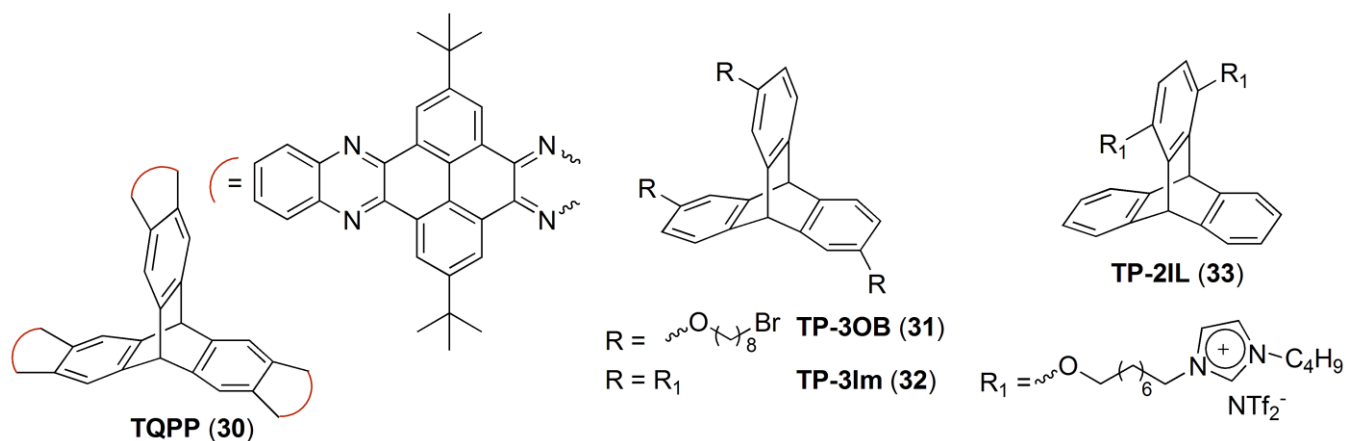


283

284 **Fig. 9.** (a) Chemical structure of propeller-like hexaphenylbenzene-based stationary phase (BT); (b) halogen bond interaction  
285 ( $\text{Cl}\cdots\pi$ ) of terminal residue of the SP with 1,3,5-trichlorobenzene.

286 Qi, Cai and co-workers reported the first example of pillar[n]arenes **37** used as a new type of  
287 stationary phase for GC separations [55]. Pillar[n]arenes are a class of macrocycle hosts made up of  
288 hydroquinone units linked by methylene bridges at the 2,5-positions, with a highly symmetrical and  
289 rigid pillar architecture and an electron-rich cavity. Also in this case, the retention behaviour and the

290 high-resolution performance towards dibromoalkanes **38** was attributed to the possibility that XB can  
291 function in this GC environment.



292 **TQPP (30)**  
293 **Fig. 10.** Structure of TP-base materials used as stationary phase for GC separations, TQPP, TP-2IL, TP-3OB, and TP-3Im.

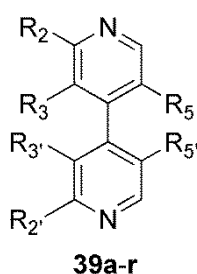
294 Finally, recently, our group also explored the possibility of XB-based GC separation [56], and  
295 retention and selectivity of polyhalogenated 4,4'-bipyridines (HBipys) **39a-r** were evaluated on  
296 Hydrodex- $\beta$ -PM (heptakis-(2,3,6-tri-O-methyl)- $\beta$ -cyclodextrin) and Chirasil Val (N-propionyl-L-valine-  
297 tert-butylamide polysiloxane) capillary columns, both containing oxygen sites as potential XB acceptors.  
298 Despite the fact that no obvious trend related to the identity of the XB emerged from the  
299 chromatographic data, the presence of iodine substituents seemed to increase retention on both columns.  
300 Moreover, the three compounds **39i**, **39o**, and **39q**, which were enantioseparated on Hydrodex- $\beta$ -PM,  
301 contained iodines.

302 It is worth noting that all XB-based mechanisms proposed until now in GC separation represent  
303 working hypotheses which were not supported by focused spectroscopic studies, calculations or analysis  
304 in the solid state. Moreover, in these studies the separation of iodinated benzenes is missing,  
305 consequently the effect of halogens on separation was only partially evaluated.

306 With the aim to tackle this unexplored question by means of a case study, we calculated  $V_{S,max}$ ,  
307  $V_{S,min}$ , and related surface parameters for HBipys **39a-r** (Table 2) and the presence of structure-GC  
308 chromatographic behaviour relationships were verified by linear regression analysis. The results

309 reported in Table 3 show a strong correlation between retention times and molecular weight (MW), area  
 310 and volume of calculated electrostatic potential surfaces, revealing a leading mechanism controlled by  
 311 the analyte shapes. On the other hand, two minor statistically significant correlations were derived  
 312 between retention time on both columns and  $V_{S,max}$  values on the halogens ( $r^2 = 0.4961$ ;  $0.4837$ , P-value  
 313 =  $0.0011$ ;  $0.0014$ ) and  $V_{S,min}$  on the nitrogen ( $r^2 = 0.4151$ ;  $0.4075$ , P-value =  $0.0039$ ;  $0.0044$ ), revealing a  
 314 possible minor contribution of both XB and hydrogen bond to retention.

315 **Table 2**  
 316 Retention times on Hydrodex- $\beta$ -PM and Chirasil-Val chiral capillary columns [56], and calculated molecular properties<sup>a</sup> of HBipys **39a-r**.



317

HBipy <b>39</b>	Substitution pattern $R_2-R_2'-R_3-R_3'-R_5-R_5'$	MW	$V_{S,max}$ (X) [kJ/mol]	$V_{S,min}$ (N) [kJ/mol]	surface area [ $\text{\AA}^2$ ]	surface volume [ $\text{\AA}^3$ ]	Hydrodex- $\beta$ -PM $t_1$ ( $t_2$ ) [min]	Chirasil-Val $t_1$ [min]
<b>a</b>	H-H-I-H-Cl-Cl	350.97	134.4	-156.9	237.9	240.4	8.82	7.60
<b>b</b>	H-H-I-H-Br-Br	439.87	131.6	-158.2	246.8	251.8	12.08	10.54
<b>c</b>	H-H-I-I-Cl-Cl	476.87	136.9	-140.4	262.3	274.6	13.43	11.79
<b>d</b>	H-H-I-I-Br-H	486.87	131.6	-158.0	253.1	262.5	15.26	13.14
<b>e</b>	H-H-I-I-Br-Br	565.77	134.1	-141.5	270.1	286.2	19.93	17.07
<b>f</b>	Cl-Cl-Br-Br-Br-Br	540.66	123.3	-131.1	285.3	299.7	24.78	20.08
<b>g</b>	Cl-Cl-I-H-Br-Br	508.76	151.3	-142.9	278.2	287.1	25.27	20.03
<b>h</b>	Cl-Cl-Cl-Cl-I-I	545.76	154.4	-128.7	292.5	309.5	29.66	23.70
<b>i</b>	Cl-Cl-I-I-Cl-Cl	545.76	154.3	-130.6	289.7	309.0	32.05 (32.65)	25.64
<b>j</b>	Cl-Cl-I-H-Br-I	555.76	151.3	-142.9	285.4	297.7	34.92	27.14
<b>k</b>	Cl-Cl-Br-Br-Br-I	587.66	153.3	-131.4	292.2	310.3	35.33	28.02
<b>l</b>	Br-Br-I-H-Br-Br	597.66	149.7	-143.6	288.1	298.5	43.53	35.02
<b>m</b>	Cl-Cl-I-H-I-I	602.76	151.8	-144.1	291.9	308.3	47.09	38.78
<b>n</b>	Cl-Cl-Br-Br-I-I	634.66	151.7	-131.6	298.7	320.6	48.10	40.35
<b>o</b>	Cl-Cl-I-I-Br-Br	634.66	151.7	-132.6	297.3	320.4	49.05 (49.70)	42.35
<b>p</b>	Br-Br-Cl-Cl-I-I	634.66	152.3	-130.3	302.4	320.8	50.27	43.32
<b>q</b>	Br-Br-I-I-Cl-Cl	634.66	150.8	-131.6	299.5	320.3	53.30 (54.10)	47.17
<b>r</b>	Br-Br-Br-Br-Br-I	676.56	149.5	-133.1	301.7	321.5	57.89	35.48

318 <sup>a</sup>Computation of electrostatic potential surfaces and related parameters were performed and graphically generated using the Spartan'10  
 319 Version 1.1.0 (Wavefunction Inc., Irvine, CA) program and employing the density functional theory (DFT) method with the B3LYP  
 320 functional and the 6-311G\* basis set.

321  
 322  
 323  
 324  
 325  
 326  
 327

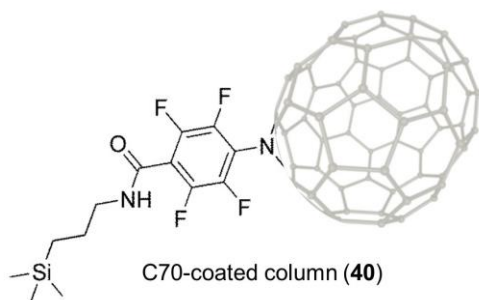
328 **Table 3**  
329 Linear regression analysis<sup>a</sup> describing the relationships between  
330 retention on Hydrodex- $\beta$ -PM and Chirasil-Val chiral capillary  
331 columns [56] and calculated molecular properties of HBipys **39a-**  
332 **r**.

Independent variable	Hydrodex- $\beta$ -PM		Chirasil-Val	
	$r^2$	P-value	$r^2$	P-value
MW	0.8595	0.0000	0.8052	0.0000
EPS area	0.8183	0.0000	0.7828	0.0000
EPS volume	0.8021	0.0000	0.7772	0.0000
max EP (X)	0.4961	0.0011	0.4837	0.0014
min (EP) (N)	0.4151	0.0039	0.4075	0.0044

333 <sup>a</sup>Statgraphics Centurion XVI (Statpoint Technologies, Inc.,  
334 Warrenton, VA, USA) was used for all linear regression analyses.

#### 335 336 4.5. Halogen bond in normal phase liquid chromatography

337 Very recently, Kubo and co-workers experimentally evaluated the strength of the X- $\pi$  interaction  
338 between carbon-materials and a series of halogenated benzenes under NP elution conditions [8],  
339 assuming that the hydrophobic interaction was completely suppressed in this environment. Under this  
340 conditions, higher retentions were observed as the number of Cl, Br, or I substituents on the benzenes  
341 increased, especially for the C70-coated column **40** (Fig. 11), which showed higher retention efficiencies  
342 than other carbon materials. In particular retention of hexahalobenzenes increased in the order F < Cl <  
343 Br < I.



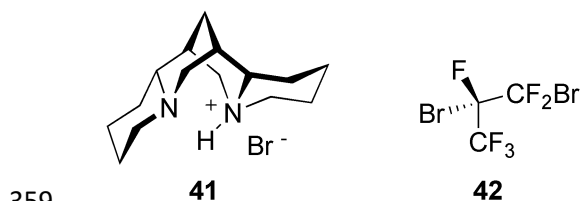
345 **Fig. 11.** Structure of the C-70 coated column **40**.

346 The carbon-materials are known to exhibit strong  $\pi$  interactions because of their many  $\pi$  electrons.  
347 By using a multidisciplinary approach based on the combined use of chromatographic analysis, UV-Vis  
348 and NMR spectroscopy, and computational calculations, the authors envisaged the existence of bimodal  
349 interactions, the  $\pi$ - $\pi$  and X- $\pi$  interactions, between the halogenated benzenes and aromatic materials.

350 **5. Halogen bond in enantioseparation science**

351 So far, XB in chiral systems has been reported in small degree, and few chiral XB donors and  
352 enantioselective processes promoted by XBs are known [9].

353 The first example in enantioseparation science dates back to 1999, when Metrangolo and Resnati  
354 used the Lewis base (-)-sparteine hydrobromide (**41**) (Fig. 12) to resolve the racemic 1,2-  
355 dibromoheptafluoropropane (**42**) [57]. The resolution occurred as a result of a highly specific inclusion of  
356 only the (*S*)-enantiomer in a chiral crystal with a helical arrangement formed by XB between the C-  
357 bound Br atoms of **42** and the Br<sup>-</sup> ions of **41**. Later, the same group performed the resolution of racemic  
358 perfluorocarbons by means of a XB-driven electron donor-acceptor recognition mechanism [58].



360 **Fig. 12.** Structure of the XB acceptor **41** and XB acceptor **42**.

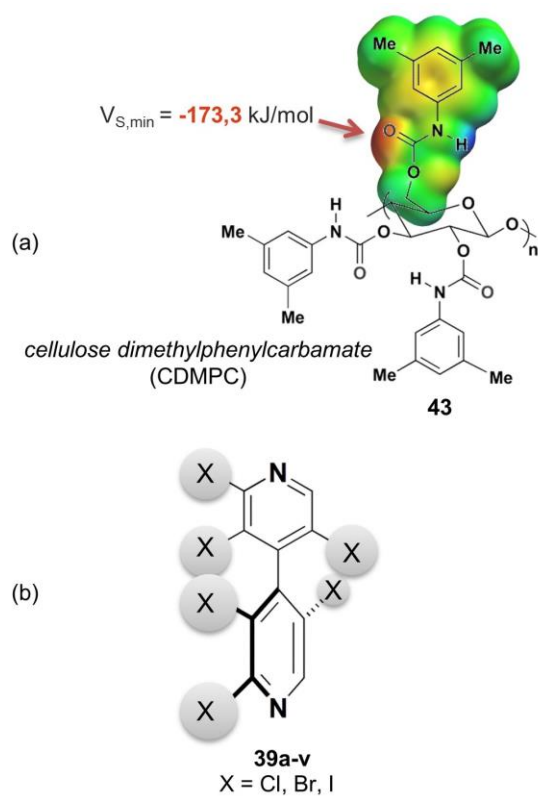
361 In the field of enantioseparation science, HPLC on chiral stationary phase is widely used. In this  
362 environment, the distinction process is based on the ability of this chiral selector to recognize the  
363 enantiomers of the analyte by means of stereoselective noncovalent interactions, which are strictly  
364 dependent on chiral selector, analyte and mobile phase.

365 In 1996, Pirkle and co-workers had highlighted an unexpected halogen effect on the HPLC  
366 enantioseparation of halogenated amide derivatives of 1-phenylethylamine [59]. Nevertheless, in this  
367 study, where Pirkle considered that “*Unexpectedly, para and meta halogen substituents increase both*  
368 *retention and enantioselectivity when nonaqueous organic mobile phases are used. The more*  
369 *polarizable the halogen, the greater the effect*”, halogen-dependent effects on enantioseparation were  
370 never explicitly related to the XB. The reason was likely due to the fact that, for a long time F, Cl, Br  
371 and I substituents in LC enantio recognition were merely considered as a Lewis base, in the perspective

372 of an isotropic distribution of the electron density [60]. On this basis, it can be expected that XB-driven  
373 enantioseparations could be recognized by means of a theoretical re-examination of some published  
374 enantioseparation processes.

375 *5.1. Enantioseparations involving XB on polysaccharide-based CSPs: a multidisciplinary approach*  
376 *integrating theoretical analysis with experiments*

377 Starting from 2014, XBs being still unexplored in HPLC enantioseparation, our group envisaged that  
378 HPLC, as a technical tool, could be successfully used to systematically investigate XBs occurring on the  
379 surface of the chiral adsorbent by properly tuning molecular properties of analyte as XB donor, selector  
380 as XB acceptor, under NP elution conditions [22,25,56].



381

382 **Fig. 13.** Chromatographic system developed for the study of XB in HPLC environment: (a) CDMPC polymer as the CSP; (b)  
383 polyhalogenated 4,4'-bipyridines as the analytes.

384

385 With this purpose, cellulose dimethylphenylcarbamate (CDMPC) **43** was selected as a chiral  
386 stationary phase (CSP) (Fig. 13a) because of a negative  $V_{S,\min}$  (-173.3 kJ/mol) which makes carbonyl  
387 functionality a good halogen  $\sigma$ -hole acceptor, similar in terms of  $V_{S,\min}$  and site structure to other typical

388 acceptors like acetone (-177.0 kJ/mol) or *N*-methylacetamide (-216.3 kJ/mol). As analytes, we have  
389 developed halogenated donors based on the electron poor 4,4'-bipyridine core (**39a-v**) (Fig. 13b) [24],  
390 where halogens serve as  $\sigma$ -hole sites, and inductors of chirality by restricted rotation around the 4,4'-  
391 bipyridyl bond. The enantioseparation of functionalized 4,4'-bipyridines being dependent on the  
392 substituents bearing by the heteroaromatic scaffold [19], the chromatographic response of the  
393 halogenated analogues is strictly dependent on the  $\sigma$ -hole depth, XB strength increasing from chlorine to  
394 bromine and iodine. Some halogenated bipyridines were studied in the solid state [24,25], and nitrogen-  
395 halogen contacts, with penetration parameters increasing from chlorine to iodine ( $-15.1$  (N $\cdots$ I)  $\leq p.p. \leq$ -  
396  $2.8$  (N $\cdots$ Cl)), were observed, these results proving the capability of these halogens to act as  $\sigma$ -hole  
397 donors.

398 To tackle the study of XB in HPLC environment, the use of distinct orthogonal techniques provides  
399 complementary information for a more comprehensive picture of XB-based enantiodistinction processes  
400 which are the result of a balanced synergy between CSP, analyte, and mobile phase. Therefore, in the  
401 last few years we have approached the question by means of a multidisciplinary study involving  
402 chromatographic analysis, X-ray diffraction analysis and theoretical calculations [22,24,56].

### 403 *5.2. Computational tools to design XB donors as test probes and rationalize related recognition* 404 *mechanisms*

405 The quantitative assessment of  $V_{S,max}$  and  $V_{S,min}$  have been found to be related to the strengths of  
406 noncovalent interactions [20,28]. In particular, the depth of  $\sigma$ -hole on halogens is related to their XB  
407 donor capability. In this regards, Murray and co-workers highlighted the importance of identifying  
408 methods and basis sets that are reliable for computing properly  $V_{S,max}$  and  $V_{S,min}$  [28]. In general too  
409 large basis sets are not needed for this purpose. Indeed, electrostatic potential values are computed for  
410 the unperturbed molecules prior to interaction in order to assess what is likely they do. On this basis,  
411 with the aim to demonstrate the concept, herein, the  $V_{S,max}$  values of three representative compounds

412 **39s-u** are reported comparing different functionals and basis set (Table 4). The relative values of the  
 413 brominated and iodinated compounds normalized with respect to the chlorinated analogue are reported  
 414 in parentheses. With all theoretical methods, the  $\sigma$ -hole on halogens increases as the atomic number of  
 415 the halogen in a comparable manner, even with the smaller basis set (DFT/B3LYP/6-311G\*), which  
 416 gives slightly more positive  $V_{S,max}$  and generates larger variations in  $\sigma$ -hole magnitude [20,28]. Indeed,  
 417 M06-2X and def2-QZVP variations of  $V_{S,max}$  on the halogen  $\sigma$ -hole are more contracted.

418 **Table 4**  
 419  $V_{S,max}$  on halogen  $\sigma$ -holes for compounds **39s-u**.



420

program/calculation level	$V_{S,max}$ [kJ/mol] <sup>a</sup>				
	CH <sub>3</sub> Cl	<b>39s</b> (X = Cl)	<b>39t</b> (X = Br)	<b>39u</b> (X = I)	iodopentafluorobenzene
Spartan <sup>b</sup> /DFT/B3LYP/6-311G*	5.9	89.9 (1.00)	119.8 (1.333)	144.2 (1.604)	164.6
Gaussian <sup>c</sup> /DFT/B3LYP/def2-QZVP	--	75.7 (1.00)	93.7 (1.238)	114.2 (1.509)	--
Gaussian <sup>c</sup> /DFT/M06-2X/def2-QZVP	--	77.9 (1.00)	93.2 (1.200)	116.1 (1.490)	--

421 <sup>a</sup>In parentheses are given the relative values of the brominated and iodinated analogues normalized with respect to the chlorinated  
 422 bipyridine **39s**.

423 <sup>b</sup>Spartan '10 Version 1.1.0 (Wavefunction Inc., Irvine, CA).

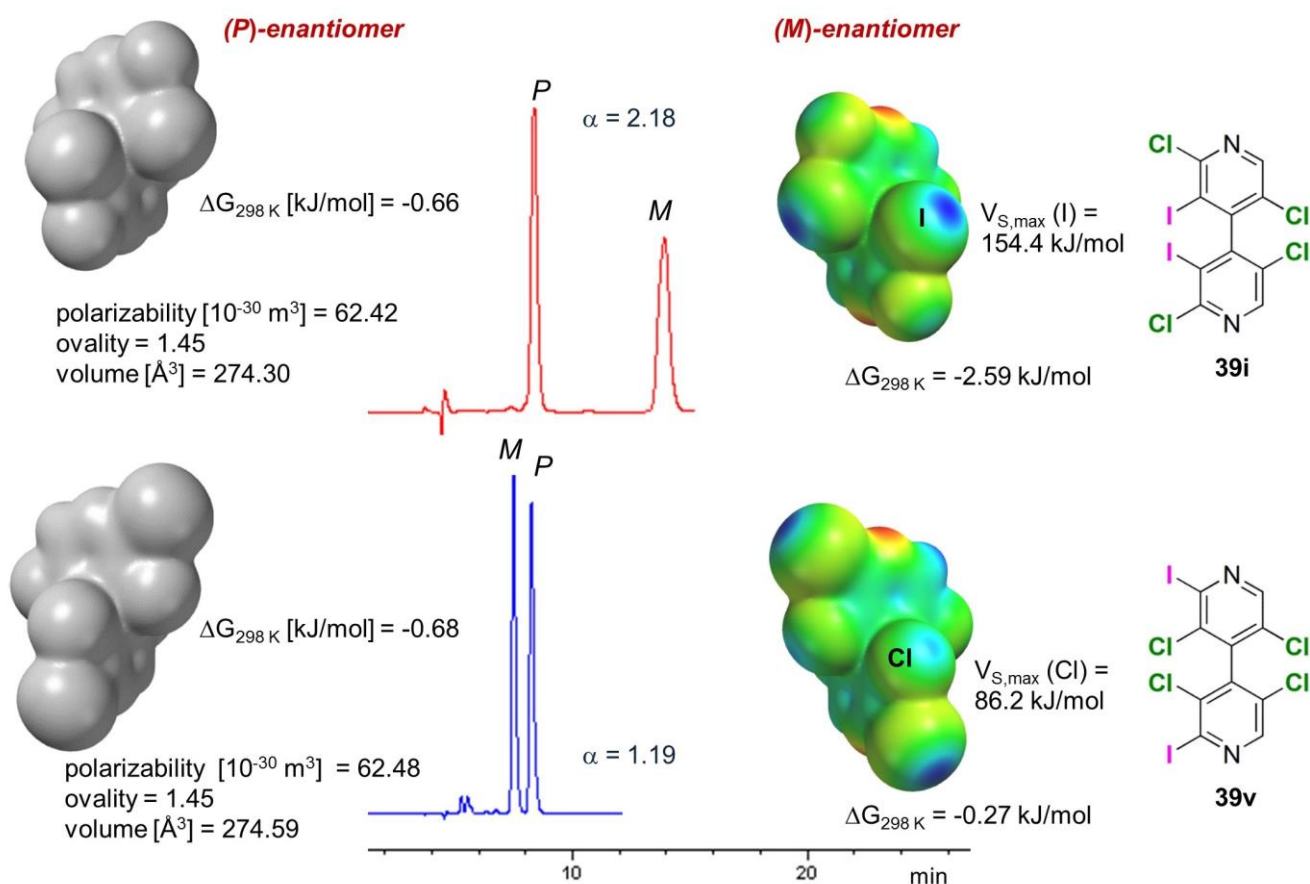
424 <sup>c</sup>Gaussian 09 (Wallingford, CT 06492, USA).

425

426 According with calculated  $V_{S,max}$  on halogens, the enantioselectivity of compounds **39a-v** on the CSP  
 427 **43** under NP elution conditions increased following the order Cl < Br < I, and  $V_{S,max}$  on iodine  
 428 substituents, ranging from 149 kJ/mol to 154 kJ/mol, were found on compounds enantioseparated with  
 429 high selectivity values ( $\alpha > 2.00$ ) [56].

430 Correlating molecular properties and experimental results allows for a better understanding of  
 431 mechanisms underlying the discrimination process. Taking into account the hydrophobic character of  
 432 halogenated compounds, two competitive mechanisms are envisaged to contribute to retention and

433 selectivity. The unreported case study described in Figure 14 has been designed and performed with the  
 434 aim to the concept.



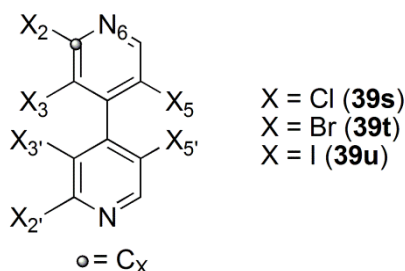
435  
 436 **Fig. 14.** Comparison of enantiorecognition mechanisms of compounds **39i** and **39v**.

437 The two *P* enantiomers of compounds **39i** and **39v** are eluted with very similar retention times and  
 438 free energy changes associated with the complex formation. This means that the retention of the *P*  
 439 enantiomers is governed by forces which are highly similar in the two enantiomers and related to their  
 440 molecular shape, thus revealing a mechanism controlled by the steric fit of the *P* stereoisomers into the  
 441 polymer groove. Differently, the *M* enantiomers show different elution times and free energy changes  
 442 which can be reasonably related to the different  $\sigma$ -hole depth around the chiral axis. Consequently, the  
 443 EEO reversal from *P,M* for **39i** to *M,P* for **39v**, is related to the fact that, for **39i**, the iodine bond-driven  
 444 mechanism is more efficient, in terms of enantiomer-CSP complex stability, compared to the

445 mechanisms based on the steric fit. On the contrary, for compound **39v**, the chlorine bond-driven  
 446 mechanism is less efficient, so the *M* stereoisomer becomes the first eluted.

447 To examine in depth the origin of the observed  $V_{S,max}$ , within a cause-effect view, we calculated the  
 448 contribution of each atom of the molecule to generate the positive  $V_{S,max}$  on the halogen (X)  $\sigma$ -holes by  
 449 means of the source function mathematical tool [61], on the basis of a theoretical methodology  
 450 (fruitfully applied by our group to the reconstruction of chalcogen  $V_{S,max}$  [31]. In Table 5, the results of  
 451 the electrostatic potential source function decomposition applied to the X-centred  $\sigma$ -holes in compounds  
 452 **39s-u** are summarized. The sign of SF is positive or negative whether the atomic source concurs or  
 453 opposes to the positive potential of  $\sigma$ -hole.

454 **Table 5**  
 455 Electrostatic potential SF decomposition of  $V_{S,max}$  at the X-centred  $\sigma$ -holes in compounds **39s-u**.



456

1	2	3	4	5	6	7	8	9
X (position)	SF% (own ring)	SF% (other ring)	SF (X)	SF (C <sub>X</sub> +X)	SF (N <sub>6</sub> )	SF (N <sub>6</sub> + C <sub>X</sub> + X)	SF [own ring – (N <sub>6</sub> +C <sub>X</sub> +X)]	$V_{S,max}$ $\sigma$ -hole [au] <sup>a</sup>
I (2)	95.3	4.7	0.071	0.109	-0.119	-0.010	0.059	0.0507
Br (2)	93.5	6.6	0.034	0.102	-0.128	-0.026	0.063	0.0403
Cl (2)	90.1	10.9	-0.006	0.093	-0.133	-0.041	0.067	0.0286
I (3)	98.7	1.9	0.081	0.048	-0.091	-0.043	0.102	0.0599
Br (3)	96.0	4.8	0.040	0.034	-0.097	-0.063	0.111	0.0498
Cl (3)	90.6	10.0	-0.003	0.018	-0.100	-0.082	0.118	0.0386
I (5)	99.1	1.6	0.076	0.039	-0.093	-0.054	0.114	0.0606
Br (5)	96.5	4.2	0.033	0.023	-0.098	-0.075	0.124	0.0501
Cl (5)	90.9	9.1	-0.010	0.006	-0.102	-0.096	0.131	0.0387

457 <sup>a</sup>Computation of electrostatic potential surfaces were performed and graphically generated using the Spartan'10 Version 1.1.0  
 458 (Wavefunction Inc., Irvine, CA) program and employing the density functional theory (DFT) method with the B3LYP functional and the 6-  
 459 311G\* basis set. Search for the exact location of  $V_{S,max}$  was made through the Multiwfn code [29] and through its module enabling  
 460 quantitative analyses of molecular surfaces [30].

461

462 This feature allows us to identify the molecular frameworks which contribute to the electrophilic  
 463 character of halogens, furnishing valuable information to design properly compounds with properties as  
 464 XB donors. Considering as reference points the  $\sigma$ -holes centred on X (*n*) (*n* = 2, 3, 5), the contribution of

465 the pyridine ring bearing X (n) is dominant (column 2) compared to the contribution of the other ring  
466 (column 3). This response was expected on the basis of the atropisomeric topology of the two orthogonal  
467 aryl planes. Moreover, the values reported in Table 5 show that the trend EP (I) > EP (Br) > EP (Cl) for  
468 the  $\sigma$ -holes (column 9) originates from a corresponding trend of the X (column 4), ( $C_X + X$ ) (column 5),  
469 and  $N_6$  (column 5) contributions which is only partly compensated by an opposite trend in the remaining  
470 ring sources (column 8). This observations highlight the pivotal role that the substituents exert on the  
471 stereoelectronic properties of the electrophilic recognition sites, guiding properly analyte design.  
472 Moreover, the different halogen contribution to the  $\sigma$ -holes of **39s** (negative) with respect to **39u**  
473 (positive) could fully justify the difference in HPLC selectivity of the two compounds ( $\alpha$ : 1.16 (**39s**),  
474 2.68 (**39u**) [25]), enantioseparation being driven by XBs on the cellulose-based CSP **43** under NP  
475 elution conditions.

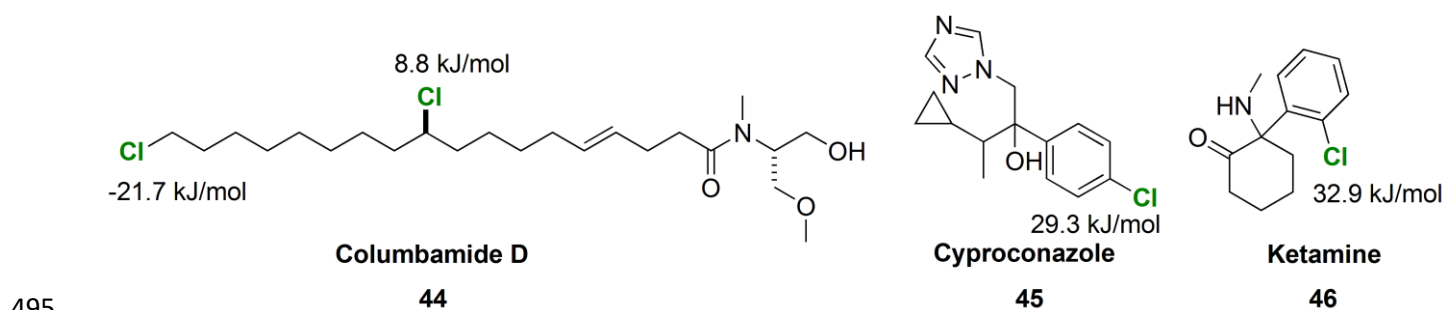
476 Finally, it is worth mentioning that also for the study of XB in HPLC environment molecular  
477 dynamics simulations [22,62] are extremely versatile to reproduce the experimental chromatographic  
478 system accounting for solvent effect and mutual conformational adjustment of analyte and selector, and  
479 to predict EEO. In particular, good agreement between experimental and simulated data was achieved by  
480 using the explicit  $\sigma$ -hole (ESH) tool [20,21] in order to account for the electrophilic character of the  
481 halogen moieties.

### 482 5.3. HPLC enantioseparations involving XB donors as analytes: a theoretical re-examination

483 In HPLC, the enantioseparations of fluorinated and chlorinated compounds are more frequent  
484 compared to those of brominated or iodinated compounds. In particular, very recently the XB has been  
485 proposed as a noncovalent interaction involved in the enantioseparation of some chlorinated compounds  
486 on polysaccharide-based CSPs. Okino and co-workers hypothesized that the enantioseparation of  
487 Columbamide D (**44**) on Chiralpak AD-H is possibly driven by a XB between chlorine on the analyte  
488 and the carbamate carbonyl group of the stationary phase [63]. On the basis of docking results, Wang

489 and co-workers proposed the occurrence of a XB between the chlorine atom on the benzene ring of  
490 Cyproconazole (**45**) and an oxygen atom on the Lux Cellulose-2 CSP [64]. Link and co-workers  
491 proposed, on the basis of docking data, the possibility of XB between the chlorine substituent of  
492 Ketamine (**46**) as an analyte and the carbonyl group of the i-Amylose-3 CSP [65].

493 In this regard, with the aim to evaluate the  $\sigma$ -hole depth on chlorines in **44-46**, we calculated the  
494  $V_{S,max}$  on chlorines at DFT level of theory (B3LYP/6-311G\*) and the results are reported in Figure 15.



496 **Fig. 15.** EP maxima on chlorine  $\sigma$ -hole in Columbamide D, Ketamine, and Cyproconazole.

497 Positive  $V_{S,max}$  values ranging from 8.8 to 32.9 kJ/mol were found, the  $V_{S,max}$  on the primary chlorine  
498 of Columbamide D being negative (-21.7 kJ/mol). On this basis, limited involvement is expected for the  
499 three compounds **44-46** as XB donors in the HPLC environment, chlorines being characterized by  
500 calculated  $V_{S,max}$  on  $\sigma$ -holes lower than 50 kJ/mol [56], and functioning in competitive systems, where  
501 hydrogen bond centres are also present as recognition sites [22].

502 The question of the possibility of fluorine to be involved in XB in LC enantioselectivity remains  
503 rather undefined [66]. Indeed, fluorine is less prone to behave as XB donor due to its high  
504 electronegativity and low polarizability, and it can act as an electrophile only when attached to strong  
505 EWGs like -CN or -F [9].

### 506 5.5 Exploiting halogen bond in enantioselectivity science: open issues and perspectives

507 In the next subsections we describe a series of new results emerging from experiments and theoretical  
508 calculations specifically designed and performed in order to assess open issues perspectives of XB  
509 utilization in (enantio)separation science.

510 5.5.1. Halogen bonds in supercritical fluid chromatography enantioseparations: possible role of CO<sub>2</sub>

511 Non-polar pressurized carbon dioxide is considered a hexane-like solvent with respect to its elution  
 512 strength [67]. Therefore, the replacement of *n*-hexane to carbon dioxide should cause no important  
 513 changes in retention and selectivity [68]. In reality, carbon dioxide is not hexane-like because it is more  
 514 polarizable, and it has local dipoles (C=O bonds) and partial charges on both carbon and oxygen [68].  
 515 Theoretical calculations and related experimental data proved that carbon dioxide can form XB-based  
 516 (O=C=O···X) associations where it acts as XB acceptor [69]. In this perspective, with the aim to verify  
 517 the chromatographic response of halogenated chiral analytes under SFC conditions, we compared  
 518 retention and selectivity of the enantiomeric pairs of compounds **39i** and **39s**, used as test probes, under  
 519 SFC (carbon dioxide/2-propanol 9:1) and NPLC (*n*-hexane/2-propanol 9:1) on CDMPC as CSP  
 520 (column: Lux Cellulose-1) in order to explore the effect of changing *n*-hexane to carbon dioxide on  
 521 retention and enantioselectivity. Under NPLC conditions, **39i** is enantioseparated with good selectivity  
 522 ( $\alpha = 2.30$ , EEO = *P,M*) through a recognition mechanism based on I···O contacts, as stereoselective  
 523 secondary interactions, iodine being a good XBD [56]. On the contrary, the selectivity value decreased  
 524 in the case of **39s** ( $\alpha = 1.22$ , EEO = *M,P*), chlorine being a poor XB donor [56]. The results of the  
 525 SFC/NPLC comparative experiments are presented in Table 6. In both cases the flow rate was 1  
 526 mL/min.

527 **Table 6**  
 528 Enantioseparation of HBipys **39i** and **39s** on CDMPC (*FR* = 1  
 529 mL/min, *T* = 25°C) under NP (*n*-hexane/2-propanol 9:1) and SFC  
 530 (carbon dioxide/2-propanol 9:1) conditions.<sup>a,b</sup>

HBipy	MP	k <sub>1</sub>	k <sub>2</sub>	$\alpha$
<b>39i</b>	NP	1.40 (1.00)	3.22 (1.00)	2.30 (1.00)
	SFC	9.82 (7.01)	14.61 (4.54)	1.49 (0.65)
<b>39s</b>	NP	0.49 (1.00)	0.60 (1.00)	1.22 (1.00)
	SFC	1.74 (3.55)	1.88 (3.13)	1.08 (0.88)

531 <sup>a</sup> Column: Phenomenex Lux 5 $\mu$  Cellulose-1 (CDMPC) 250 x 4.6  
 532 mm. Detection wavelength, 220 nm.

533 <sup>b</sup>In parentheses are given the relative values of SFC  
 534 chromatographic parameters normalized with respect to NPLC  
 535 parameters.

536

537 For both racemates **39i** and **39s**, SFC conditions displayed lower eluotropic power than NPLC  
538 conditions, retention factors being from four to seven times higher in SFC than in HPLC, with retention  
539 increment higher for **39i** compared to **39s**. Indeed, for compound **39i**, NPLC condition produced  
540 baseline resolution within 12 minutes, whereas SFC conditions yielded a longer 50 minutes analysis, at  
541 the same  $T = 25^{\circ}\text{C}$ . Differently, analysis time increase was not so pronounced for compound **39s**  
542 (elution time: normal phase, 5 min; SFC, 9 min). On this basis, polyhalogenated analytes as XB donors  
543 show stronger retention in SFC. Taking into account that on the CDMPC the carbonyls are acceptors for  
544 both XB donors and hydrogen bond donors, our results are consistent with the fact that the interaction  
545 ability of CDMPC toward hydrogen bond donors was reported to be stronger in SFC with respect to  
546 NPLC [68].

547 Both enantiomer pairs **39i** and **39s** were eluted in SFC keeping unchanged NPLC EEO. However, a  
548 decrease of selectivity for both analytes (**39i**, -37%; **39s**, -12%) was observed in SFC compared to  
549 NPLC, due to a different effect of carbon dioxide on the retention of the second eluted enantiomers  
550 compared to the first eluted. Indeed, for the two second eluted enantiomers, the retention increase,  
551 moving from NPLC to SFC conditions, is lower (4.54 and 3.13 times longer for **39i** and **39s**,  
552 respectively) than the retention increase of the first eluted enantiomers (7.01 and 3.55 times longer for  
553 **39i** and **39s**, respectively). In particular, for **39i**, the effect is higher resulting in a higher decrease of  
554 selectivity compared to **39s**.

555 At the molecular level, the same effect on both enantiomers could be expected if the  $\text{CO}_2$  acts as *n*-  
556 hexane (non-interacting solvent). On the contrary, according with the experimental data, a different  
557 effect of  $\text{CO}_2$  is foreseeable if it associates with halogens, reasonably forming XB-based solvation  
558 clusters. In this context, halogens are less prone to be involved in XB with the CSP, thus the presence of  
559  $\text{CO}_2$  is more detrimental for **39i** which forms stronger XBs.

560 On this basis, further investigations are needed to confirm these preliminary observations on the  
561 potential role of carbon dioxide in XB-based SFC recognition processes, a question so far unexplored.

562 5.5.2. Potential function of halogenated polysaccharide-based CSPs as XBDs: a theoretical examination

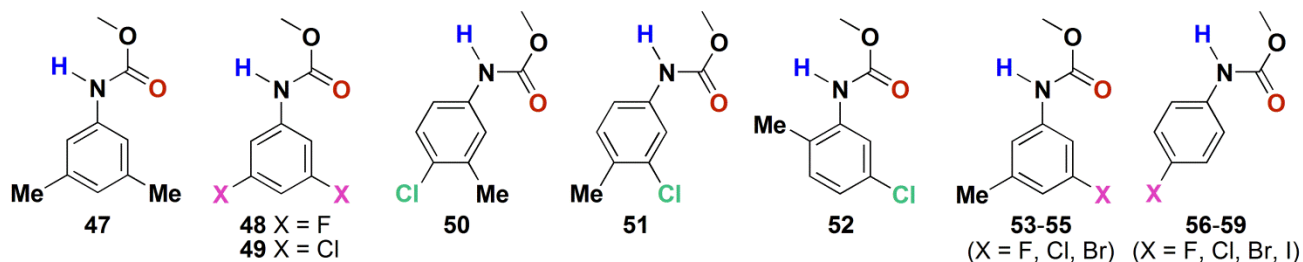
563 Polysaccharide carbamates-based CSPs are the most used for HPLC enantioseparations [70]. The  
564 polysaccharide backbone is the essential element of this polymeric system, with the conformational  
565 chirality depending on the peculiar helical twist generated by specific glycosidic linkages in cellulose  
566 and amylose polymeric chains [70,71]. Significantly, the polymer backbone is functionalized with a  
567 polar layer containing carbamate moieties able to exert polar interactions and located inside the polymer  
568 groove, and a hydrophobic layer containing substituted aromatic rings, located outside the polymer  
569 groove and able to activate  $\pi$ - $\pi$  interactions (Fig. 13a) with analytes. Nowadays, different types of  
570 polysaccharide-based CSPs are commercially available, and the side chains are characterized by  
571 distinctive steric and electronic properties which are the key to the different selectivity of the  
572 corresponding CSPs. Indeed, the electronic properties of the polar layer and its ability to exert HBs are  
573 tuned by changing type and position of both alkyl- and chloro substituents onto the terminal aromatic  
574 ring [70,72]. On the other hand, studies on fluorinated, brominated and iodinated CSPs were published  
575 [73,74] in the late twentieth century.

576 Until recently, no systematic study has been performed about the possible electrophilic behaviour of  
577 the chlorine located on polysaccharide-based CSPs. However, some authors speculated that XB could  
578 underlie recognition mechanisms on chlorinated CSPs. In this regard, West and co-workers stated  
579 *“Halogen bonds should also be considered as possible contributors to the specific retention and*  
580 *separation behavior of chlorinated CSP”* [75], and later Jiang and co-workers considered *“the halogen*  
581 *bonding occurred as an intermolecular interaction when chlorine atom acted as an electron density*  
582 *acceptor (Lewis acid) and tended to interact with electron donor partners. In this regard, the chlorine*  
583 *atom on CSP phenyl can interact with the C=O group and phenyl ring of the enantiomer by halogen-*  
584 *carbonyl oxygen and halogen- $\pi$  interactions, respectively. Based on the above reasons, both the*

585 *electron-withdrawing inductive effect and the halogen bonding produced by chlorine atoms of CSP*  
 586 *appeared to be favorable for the enantioseparation” [76].*

587 **Table 7**

588 Calculated  $V_{S,max}$  and  $V_{S,min}$  [kJ/mol] on carbamate N-H and C=O, respectively, and  $V_{S,max}$  [kJ/mol] on halogen (X)  $\sigma$ -holes of substituted  
 589 phenylcarbamate side chain **47-59**.



side chain (Ar substituents)	$V_{S,max}$ N-H	$V_{S,min}$ C=O	$V_{S,max}$ X ( $\sigma$ -hole)	CSP (Ar substituents)	$V_{S,max}$ N-H	$V_{S,min}$ C=O	$V_{S,max}$ X ( $\sigma$ -hole)
<b>47</b> (3,5-diMe)	206.8	-173.3	--	<b>54</b> (3-Cl,5-Me)	228.6	-155.9	26.9 (Cl)
<b>48</b> (3,5-diF)	243.2	-151.9	-68.7 (F)	<b>55</b> (3-Br,5-Me)	229.2	-156.4	61.9 (Br)
<b>49</b> (3,5-diCl)	249.5	-147.3	41.4 (Cl)	<b>56</b> (4-F)	228.5	-161.5	-81.5 (F)
<b>50</b> (4-Cl,3-Me)	231.6	-156.5	20.0 (Cl)	<b>57</b> (4-Cl)	235.3	-155.5	22.7 (Cl)
<b>51</b> (3-Cl,4-Me)	227.9	-159.2	27.7 (Cl)	<b>58</b> (4-Br)	235.5	-155.7	57.5 (Br)
<b>52</b> (5-Cl,2-Me)	209.5	-162.3	12.0 (Cl)	<b>59</b> (4-I)	236.3	-154.9	87.8 (I)
<b>53</b> (3-F,5-Me)	225.9	-159.8	-77.4 (F)				

591

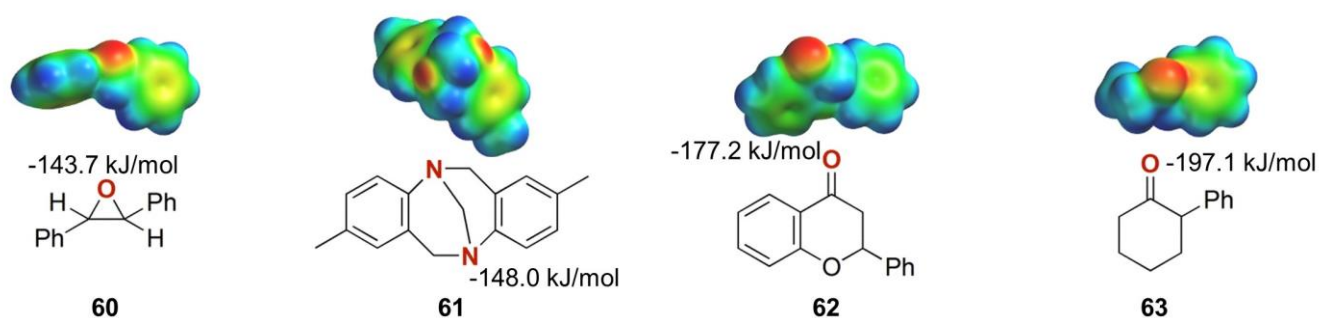
592 We report herein a theoretical examination of the electronic properties of some halogenated side  
 593 chains associated with commercially available CSPs (Table 7, side chains **47**, **49-52**, **54**, **57**) or reported  
 594 in the literature with respect to their preparation and enantioseparation performances (side chains **48**, **53**,  
 595 **55**, **56**, **58**, **59**). For each side chain, we calculated (DFT/B3LYP/6-311G\*) the  $V_{S,max}$  and  $V_{S,min}$  on  
 596 carbamate N-H and CO, respectively, as an indicator of their capability as hydrogen bond donor and  
 597 acceptor. In addition, the  $V_{S,max}$  on halogen  $\sigma$ -holes were considered in order to get a quantitative  
 598 estimation of the capability of the halogens as electrophilic XB donors.

599 The following observations emerged:

600 1) as expected, fluorine, as substituent of the phenylcarbamates, does not present a  $\sigma$ -hole with  
 601 positive  $V_{S,max}$  and negative values of  $V_{S,max}$  ranging from -81.5 kJ/mol to -61.4 kJ/mol were calculated  
 602 for side chains **48**, **53** and **56**. Therefore, in principle, for the corresponding CSPs XB cannot underlie  
 603 retention and enantioselectivity;

604 2) in the case of chlorine, positive  $V_{S,max}$  values ranging from 12.0 kJ/mol to 41.4 kJ/mol revealed the  
 605 presence of electrophilic  $\sigma$ -holes on halogens, but small in magnitude. On this basis, the potential of  
 606 these chlorines to be involved in XB is rather limited, in particular considering that the corresponding N-  
 607 H moieties (side chains **49-52**, **54** and **57**), are competitive sites, showing higher positive  $V_{S,max}$  (209.5  
 608 kJ/mol  $\leq$  EP<sub>N-H</sub>  $\leq$  249.5 kJ/mol). Therefore, it is likely that analytes with properties as XB and hydrogen  
 609 bond acceptors show a preference towards N-H, which is more electrophilic as recognition site;

610 3) higher positive  $V_{S,max}$  were calculated for bromine in side chains **55** and **58**, and as expected, the  
 611 highest positive EP value was found for iodine in the side chain **59**;



612 **60** **61** **62** **63**  
 613 **Fig. 16.** EP minima on O or N as nucleophilic recognition sites in compounds **60-63**.

614 4) from a re-examination of some chromatographic results reported by Okamoto and co-workers [73],  
 615 an interesting trend was observed in the comparative retention of four chiral compounds containing XB  
 616 acceptors as recognition sites, namely *trans*-stilbene oxide (**60**), Tröger base (**61**), flavanone (**62**) and 2-  
 617 phenylcyclohexanone (**63**) (Fig. 16), on the cellulose-based CSPs containing 4-halophenyl side chains  
 618 **56-59**. Indeed, for this series of analytes, the retention factors of the first eluted enantiomers increase as  
 619 the  $V_{S,min}$  on the nucleophilic recognition sites (**60** < **61** < **62** < **63**) only with the iodinated **59**-containing  
 620 CSP, whereas a different trend (**60** < **61** < **63** < **62**) was observed on the other three cellulose-based  
 621 CSPs. Moreover, it is worth noting an EEO reversal for **62** by changing **56-58**-containing CSPs  
 622 (enantiomer (+)) to the iodinated **59**-containing CSP (enantiomer (-)).

623 Two pieces of information emerge from this theoretical examination: *a*) the presence of halogen in  
 624 CSP structures does not mean that XB underlies enantiomer distinction and the magnitude of the  $\sigma$ -hole

625 should be always evaluated theoretically; *b*) the potential function of iodine as XB donor (electrophile)  
626 on polysaccharide-based CSPs deserves to be considered in the next future.

## 627 **6. Conclusions and perspectives**

628 The studies published so far have shown that XBs can promote separation processes, where halogens  
629 behave as electrophilic descriptors. This aspect is of particular relevance in pharmaceutical,  
630 environmental and industrial analyses where the separation of halogenated compounds is not unusual.  
631 Nevertheless, the study of XB in separation science is still in its infancy and further investigations are  
632 needed in order to find new evidences and make the concept familiar also in this field. For this purpose,  
633 a balanced synergy between experimental, theoretical methods and techniques is the best tool to set up  
634 appropriate hypotheses and achieve reliable conclusions.

635 In particular, a growing number of highly directional bromine and iodine-oxygen contacts have been  
636 evidenced in biological, medicinal and pharmaceutical chemistry, proving the potential of halogen  
637 substituents to contribute to ligand binding through XB [11]. On this basis, in the next future an  
638 increasing interest towards compounds containing electrophilic halogen  $\sigma$ -holes is expected in drug  
639 discovery and pharmaceutical chemistry. In this perspective, XB as a noncovalent interaction represents  
640 a pivotal tool for separation and enantioseparation of pharmaceuticals containing electrophilic holes as  
641 recognition sites. Interestingly, the discovery of the first halogen bond-driven self-disproportionation of  
642 enantiomers has been recently reported [77].

643 On the other hand, other interactions involving electrophilic  $\sigma$ -holes could function in separation  
644 science. In this regards, recent experiments and calculations have also paved the way for chalcogen and  
645  $\pi$ -hole bonds application in separation science [31,78].

## 646 **Acknowledgements**

647 This work has been partially supported by Università Ca' Foscari Venezia, Italy (Dipartimento di  
648 Scienze Molecolari e Nanosistemi DSMN, ADIR funds). P.P. sincerely thanks Prof. Bezhan  
649 Chankvetadze (Tbilisi State University, Georgia) for valuable and stimulating discussions.

## 650 **References**

- 651 [1] M.T. Bowser, D.D.Y. Chen, Recent developments towards a unified theory for separation science,  
652 *Electrophoresis* 19 (1998) 1586-1589.
- 653 [2] G. Guiochon, L.A. Beaver, Separation science is the key to successful biopharmaceuticals, *J.*  
654 *Chromatogr. A* 1218 (2011) 8836-8858.
- 655 [3] N.L. Kuehnbaum, P. Britz-McKibbin, New advances in separations for metabolomics: resolving  
656 chemical diversity in a post-genomic era, *Chem. Rev.* 113 (2013) 2437-2468.
- 657 [4] H.J. Schneider, Binding mechanisms in supramolecular complexes, *Angew. Chem. Int. Ed.* 48  
658 (2009) 3924–3977.
- 659 [5] H.J. Schneider, Quantification of noncovalent interactions - Promises and problems, *New J. Chem.*  
660 43 (2019) 15498-15512..
- 661 [6] J.M. Lehn, Supramolecular chemistry – Scope and perspectives, molecules, supermolecules, and  
662 molecular devices, *Angew. Chem. Int. Ed.* 27 (1988) 89–112.
- 663 [7] A.S. Mahadevi, G.N. Sastry, Cooperativity in noncovalent interactions, *Chem. Rev.* 116 (2016)  
664 2775–2825.
- 665 [8] E. Kanao, T. Morinaga, T. Kubo, T. Naito, T. Matsumoto, T. Sano, H. Maki, M. Yan, K. Otsuka,  
666 Separation of halogenated benzenes enabled by investigation of halogen– $\pi$  interactions with  
667 carbon materials, *Chem. Sci.* (2020) DOI: 10.1039/c9sc04906a.
- 668
- 669 [9] G. Cavallo, P. Metrangolo, R. Milani, T. Pilati, A. Priimagi, G. Resnati, G. Terraneo, The halogen  
670 bond, *Chem. Rev.* 116 (2016) 2478–2601.
- 671 [10] P.J. Costa, The halogen bond: nature and applications, *Phys. Sci. Rev.* (2017) 20170136.

- 672 [11] R. Wilcken, M.O. Zimmermann, A. Lange, A.C. Joerger, F.M. Boeckler, Principles and  
673 applications of halogen bonding in medicinal, chemistry and chemical biology, *J. Med. Chem.* 56  
674 (2013) 1363–1388.
- 675 [12] X.Q. Yan, Q.J. Shen, X.R. Zhao, H.Y. Gao, X. Pang, W.J. Jin, Halogen bonding: a new retention  
676 mechanism for the solid phase extraction of perfluorinated iodoalkanes, *Anal. Chim. Acta* 753  
677 (2012) 48–56.
- 678 [13] A.B. Lara, C. Caballo, M.D. Sicilia, S. Rubio, Halogen bonding for increasing efficiency in liquid-  
679 liquid microextraction: application to the extraction of hexabromocyclododecane enantiomers in  
680 river water, *J. Chromatogr. A* 1600 (2019) 95–104.
- 681 [14] Q. Zhang, M. Qi, J. Wang, Star-shaped oligothiophene-functionalized truxene materials as  
682 stationary phases for capillary gas chromatography, *J. Chromatogr. A* 1525 (2017) 152–160.
- 683 [15] L. Yu, J. He, M. Qi, X. Huang, Amphiphilic triptycene-based stationary phase for high-resolution  
684 gas chromatographic separation, *J. Chromatogr. A* 1599 (2019) 239–246.
- 685 [16] T. Takeuchi, Y. Minato, M. Takase, H. Shinmori, Molecularly imprinted polymers with halogen  
686 bonding-based molecular recognition sites, *Tetrahedron Lett.* 46 (2005) 9025–9027.
- 687 [17] M. Lämmerhofer, Chiral recognition by enantioselective liquid chromatography: mechanisms and  
688 modern chiral stationary phases, *J. Chromatogr. A* 1217 (2010) 814–856.
- 689 [18] G.K.E. Scriba, Chiral recognition in separation sciences. Part I: Polysaccharide and cyclodextrin  
690 selectors, *Trends in Anal. Chem.* 120 (2019) 115639.
- 691 [19] P. Peluso, V. Mamane, E. Aubert, S. Cossu, Insights into the impact of shape and electronic  
692 properties on the enantioseparation of polyhalogenated 4,4'-bipyridines on polysaccharide-type  
693 selectors. Evidence of stereoselective halogen bonding interactions, *J. Chromatogr. A* 1345 (2014)  
694 182–192.
- 695 [20] M.H. Kolář, P. Hobza, Computer modeling of halogen bonds and other  $\sigma$ -hole interactions, *Chem.*  
696 *Rev.* 116 (2016) 5155–5187.

- 697 [21] R. Nunes, D. Vila-Viçosa, P.J. Costa, Tackling halogenated species with PBSA: effect of  
698 emulating the  $\sigma$ -hole, *J. Chem. Theory Comput.* 15 (2019) 4241–4251.
- 699 [22] R. Dallochio, A. Dessì, M. Solinas, A. Arras, S. Cossu, E. Aubert, V. Mamane, P. Peluso,  
700 Halogen bond in high-performance liquid chromatography enantioseparations: description,  
701 features and modelling, *J. Chromatogr. A* 1563 (2018) 71–81.
- 702 [23] A.C.C. Carlsson, A.X. Veiga, M. Erdélyi, Halogen bonding in solution, *Top. Curr. Chem.* 359  
703 (2015) 49–76.
- 704 [24] V. Mamane, P. Peluso, E. Aubert, S. Cossu, P. Pale, Chiral hexalogenated 4,4'-bipyridines, *J. Org.*  
705 *Chem.* 81 (2016) 4576–4587.
- 706 [25] P. Peluso, V. Mamane, R. Dallochio, A. Dessì, R. Villano, D. Sanna, E. Aubert, P. Pale, S.  
707 Cossu, Polysaccharide-based chiral stationary phases as halogen bond acceptors: a novel strategy  
708 for detection of stereoselective  $\sigma$ -hole bonds in solution, *J. Sep. Sci.* 41 (2018) 1247–1256.
- 709 [26] Y. Shao, L.F. Molnar, Y. Jung, J. Kussmann, C. Ochsenfeld, S.T. Brown, A.T.B. Gilbert, L.V.  
710 Slipchenko, S.V. Levchenko, D.P. O'Neil, R.A. Di Stasio Jr, R.C. Lochan, T. Wang, G.J.O. Beran,  
711 N.A. Besley, J.M. Herbert, C.Y. Lin, T. VanVoorhis, S.H. Chien, A. Sodt, R.P. Steele, V.A.  
712 Rassolov, P.E. Maslen, P.P. Korambath, R.D. Adamson, B. Austin, J. Baker, E.F.C. Byrd, H.  
713 Dachsel, R.J. Doerksen, A. Dreuw, B.D. Dunietz, A.D. Dutoi, T.R. Furlani, S.R. Gwaltney, A.  
714 Heyden, S. Hirata, C.-P. Hsu, G. Kedziora, R.Z. Khalliulin, P. Klunzinger, A.M. Lee, M.S. Lee,  
715 W.Z. Liang, I. Lotan, N. Nair, B. Peters, E.I. Proynov, P.A. Pieniazek, Y.M. Rhee, J. Ritchie, E.  
716 Rosta, C.D. Sherrill, A.C. Simmonett, J.E. Subotnik, H.L. Woodcock III, W. Zhang, A.T. Bell,  
717 A.K. Chakraborty, D.M. Chipman, F.J. Keil, A. Warshel, W.J. Hehre, H.F. Schaefer, J. Kong, A.I.  
718 Krylov, P.M.W. Gill, M. Head-Gordon, Advances in methods and algorithms in a modern  
719 quantumchemistry program package, *Phys. Chem. Chem. Phys.* 8 (2006) 3172–3191.
- 720 [27] M.J. Frisch, G.W. Trucks, H.B. Schlegel, G.E. Scuseria, M.A. Robb, J.R. Cheeseman, G.  
721 Scalmani, V. Barone, B. Mennucci, G.A. Petersson, H. Nakatsuji, M. Caricato, X. Hratchian, H.P.

722 Li, A.F. Izmaylov, J. Bloino, G. Zheng, J.L. Sonnenberg, M. Hada, M. Ehara, K. Toyota, R.  
723 Fukuda, J. Hasegawa, M. Ishida, T. Nakajima, Y. Honda, O. Kitao, H. Nakai, T. Vreven, J.A.  
724 Montgomery Jr., J.E. Peralta, F. Ogliaro, M. Bearpark, J.J. Heyd, E. Brothers, K.N. Kudin, V.N.  
725 Staroverov, T. Keith, R. Kobayashi, J. Normand, K. Raghavachari, A. Rendell, J.C. Burant, S.S.  
726 Iyengar, J. Tomasi, M. Cossi, N. Rega, J.M. Millam, M. Klene, Inc. Gaussian, C.T. Wallingford, et  
727 al., Gaussian 09, Revision B. 01 (2010).

728 [28] K.E. Riley, K.-A. Tran, P. Lane, J.S. Murray, P. Politzer, Comparative analysis of electrostatic  
729 potential maxima and minima on molecular surfaces, as determined by three methods and a variety  
730 of basis sets, *J. Comput. Sci.* 17 (2016) 273-284.

731 [29] T. Lu, F. Chen, Multiwfn: a multifunctional wavefunction analyzer, *J. Comp. Chem.* 33 (2012)  
732 580–592.

733 [30] T. Lu, F. Chen, Quantitative analysis of molecular surface based on improved marching tetrahedra  
734 algorithm, *J. Mol. Graph. Model.* 38 (2012) 314–323.

735 [31] P. Peluso, C. Gatti, A. Dessì, R. Dallochio, R. Weiss, E. Aubert, P. Pale, S. Cossu, V. Mamane,  
736 Enantioseparation of fluorinated 3-arylthio-4,4'-bipyridines: insights into chalcogen and  $\pi$ -hole  
737 bonds in high-performance liquid chromatography, *J. Chromatogr. A* 1567 (2018) 119–129.

738 [32] M. Colin, Note sur quelques combinaisons de l'iode, *Ann. Chim.* 91 (1814) 252-272.

739 [33] F. Guthrie, On the iodide of iodammonium, *J. Chem. Soc.* 16 (1863) 239-244.

740 [34] R.A. Zingaro, M. Hedges, Phosphine oxide-halogen complexes: effect on P-O and P-S stretching  
741 frequencies, *J. Phys. Chem.* 65 (1961) 1132-1138.

742 [35] H. Bent, Structural chemistry of donor-acceptor interactions, *Chem. Rev.* 68 (1968) 587-648.

743 [36] O. Hassel, Structural aspects of interatomic charge-transfer bonding, *Science* 170 (1970) 497-502.

744 [37] G.R. Desiraju, P. Shing Ho, L. Kloo, A.C. Legon, R. Marquardt, P. Metrangolo, P. Politzer, G.  
745 Resnati, K. Rissanen, Definition of the halogen bond (IUPAC recommendations 2013), *Pure Appl.*  
746 *Chem.* 85 (2013) 1711–1713.

- 747 [38] T. Brinck, J.S. Murray, P. Politzer, Surface electrostatic potentials of halogenated methanes as  
748 indicators of directional intermolecular interactions, *Int. J. Quantum Chem.* 44 (1992) 57–64.
- 749 [39] T. Clark, M. Hennemann, J.S. Murray, P. Politzer, Halogen bonding: the  $\sigma$ -hole, *J. Mol. Model.* 13  
750 (2007) 291–296.
- 751 [40] P. Politzer, J.S. Murray, T. Clark, Halogen bonding and other  $\sigma$ -hole interactions: a perspective,  
752 *Phys. Chem. Chem. Phys.* 15 (2013) 11178-11189.
- 753 [41] A. Bondi, van der Waals volumes and radii, *J. Phys Chem.* 68 (1964) 441–451.
- 754 [42] T. Brinck, J.H. Stenlid, The molecular surface property approach: a guide to chemical interactions  
755 in chemistry, medicine, and material science, *Adv. Theory Simul.* 2 (2019) 1800149.
- 756 [43] H. Wang, W. Wang, W. J. Jin,  $\sigma$ -Hole bond vs  $\pi$ -hole bond: a comparison based on halogen bond  
757 *Chem. Rev.* 116 (2016) 5072-5104.
- 758 [44] J. Andrés, P.W. Ayers, R.A. Boto, R. Carbó-Dorca, H. Chermette, J. Cioslowski, J. Contreras-  
759 García, D.L. Cooper, G. Frenking, C. Gatti, F. Heidar-Zadeh, L. Joubert, A. Martín Pendás, E.  
760 Matito, I. Mayer, A.J. Misquitta, Y. Mo, J. Pilmé, P.L.A. Popelier, M. Rahm, E. Ramos-Cordoba,  
761 P. Salvador, W.H. Eugen Schwarz, S. Shahbazian, B. Silvi, M. Solà, K. Szalewicz, V. Tognetti, F.  
762 Weinhold, É.-L. Zins, Nine questions on energy decomposition analysis, *J. Comput. Chem.* 40  
763 (2019) 2248-2283.
- 764 [45] T. Clark, Halogen bonds and  $\sigma$ -holes, *Faraday Discuss.* 203 (2017) 9-27.
- 765 [46] P. Metrangolo, Y. Carcenac, M. Lahtinen, T. Pilati, K. Rissanen, A. Vij, G. Resnati, Nonporous  
766 organic solids capable of dynamically resolving mixtures of diiodoperfluoroalkanes, *Science* 323  
767 (2009) 1461-1464.
- 768 [47] C. Li, L. Li, X. Yang, W. J. Jin, Halogen bonding-assisted adsorption of iodoperfluoroarenes on a  
769 strong anion exchanger and its potential application in solid-phase extraction, *Colloids and*  
770 *surfaces A: Physicochem. Eng. Aspects* 520 (2017) 497–504.

- 771 [48] A. Ballesteros-Gómez, L. Lunar, M.D. Sicilia, S. Rubio, Hyphenating supramolecular solvents  
772 and liquid chromatography: tips for efficient extraction and reliable determination of organics,  
773 *Chromatographia* 82 (2019) 111-124.
- 774 [49] A.B. Lara, C. Caballo, M.D. Sicilia, S. Rubio, Speeding up the extraction of  
775 hexabromocyclododecane enantiomers in soils and sediments based on halogen bonding, *Anal.*  
776 *Chim. Acta* 1027 (2018) 47-56.
- 777 [50] A.B. Lara, C. Caballo, M.D. Sicilia, S. Rubio, Enantiomer-specific determination of  
778 hexabromocyclododecane in fish by supramolecular solvent-based single-step sample treatment  
779 and liquid chromatography–tandem mass spectrometry, *Anal. Chim. Acta* 752 (2012) 62-68.
- 780 [51] Q. Lv, S. Feng, L. Jing, Q. Zhang, M. Qi, J. Wang, H. Bai, R. Fu, Features of a truxene-based  
781 stationary phase in capillary gas chromatography for separation of some challenging isomers, *J.*  
782 *Chromatogr. A* 1454 (2016) 114-119.
- 783 [52] Y. Yang, Z. Chang, X. Yang, M. Qi, J. Wang, Selectivity of hexaphenylbenzene-based  
784 hydrocarbon stationary phase with propeller-like conformation for aromatic and aliphatic isomers,  
785 *Anal. Chim. Acta* 1016 (2018) 69-77.
- 786 [53] Y. Yang, Q. Wang, M. Qi, X. Huang,  $\pi$ -Extended triptycene-based material for capillary gas  
787 chromatographic separations, *Anal. Chim. Acta* 988 (2017) 121-129.
- 788 [54] J. He, L. Yu, X. Huang, M. Qi, Triptycene-based stationary phases for gas chromatographic  
789 separations of positional isomers, *J. Chromatogr. A* 1599 (2019) 223-230.
- 790 [55] Y. Zhang, Q. Lv, M. Qi, Z. Cai, Performance of permethyl pillar[5]arene stationary phase for  
791 high-resolution gas chromatography, *J. Chromatogr. A* 1496 (2017) 115-121.
- 792 [56] P. Peluso, V. Mamane, E. Aubert, A. Dessì, R. Dallochio, A. Dore, P. Pale, S. Cossu, Insights  
793 into halogen bond-driven enantioseparations, *J. Chromatogr. A* 1467 (2016) 228–238.

- 794 [57] A. Farina, S.V. Meille, M.T. Messina, P. Metrangolo, G. Resnati, G. Vecchio, Resolution of  
795 racemic 1,2-dibromohexafluoropropane through halogen-bonded supramolecular helices, *Angew.*  
796 *Chem. Int. Ed.* 38 (1999) 2433-2436.
- 797 [58] M.T. Messina, P. Metrangolo, G. Resnati, Resolution of racemic perfluorocarbons through self-  
798 assembly driven by electron donor-acceptor intermolecular recognition, *ACS Symp. Ser.* 746  
799 (2000) 239–254.
- 800 [59] W.H. Pirkle, K.Z. Gan, L.J. Brice, The enhancement of enantioselectivity by halogen substituents,  
801 *Tetrahedron: Asymmetry* 7 (1996) 2813–2816.
- 802 [60] P. Peluso, V. Mamane, S. Cossu, Liquid chromatography enantioseparations of halogenated  
803 compounds on polysaccharide-based chiral stationary phases: role of halogen substituents in  
804 molecular recognition, *Chirality* 27 (2015) 667–684.
- 805 [61] C. Gatti, F. Cargnoni, L. Bertini, Chemical information from the source function, *J. Comput.*  
806 *Chem.* 24 (2003) 422-436.
- 807 [62] P. Peluso, A. Dessì, R. Dallochio, V. Mamane, S. Cossu, Recent studies of docking and  
808 molecular dynamics simulation for liquid-phase enantioseparations, *Electrophoresis* 40 (2019)  
809 1881–1896.
- 810 [63] J.A.V. Lopez, J.G. Petitbois, C.S. Vairappan, T. Umezawa, F. Matsuda, T. Okino, Columbamides  
811 D and E: chlorinated fatty acid amides from the marine cyanobacterium *Moorea bouillonii*  
812 collected in Malaysia, *Org. Lett.* 19 (2017) 4231–4234.
- 813 [64] Z. He, F. Wu, W. Xia, L. Li, K. Hu, A.E. Kaziem, M. Wang, Separation and detection of  
814 cyproconazole enantiomers and its stereospecific recognition with chiral stationary phase by high-  
815 performance liquid chromatography, *Analyst* 144 (2019) 5193-5200.
- 816 [65] R.K. Hofstetter, F. Potlitz, L. Schulig, S. Kim, M. Hasan, A. Link, Subcritical fluid  
817 chromatography at sub-ambient temperatures for the chiral resolution of ketamine metabolites  
818 with rapid-onset antidepressant effects, *Molecules* 24 (2019) 1927.

- 819 [66] K. Eskandari, M. Lesani, Does fluorine participate in halogen bonding?, *Chem. Eur. J.* 21 (2015)  
820 4739–4746.
- 821 [67] D. Speybrouck, E. Lipka, Preparative supercritical fluid chromatography: a powerful tool for  
822 chiral separations, *J. Chromatogr. A* 1467 (2016) 33-55.
- 823 [68] S. Khater, M.A. Lozac'h, I. Adam, E. Francotte, C. West, Comparison of liquid and supercritical  
824 fluid chromatography mobile phases for enantioselective separations on polysaccharide stationary  
825 phases, *J. Chromatogr. A* 1467 (2016) 463-472.
- 826 [69] X. Zhu, Y. Lu, C. Peng, J. Hu, H. Liu, .Y. Hu, Halogen bonding interactions between brominated  
827 ion pairs and CO<sub>2</sub> molecules: implications for design of new and efficient ionic liquids for CO<sub>2</sub>  
828 absorption, *J. Phys. Chem. B* 115 (2011) 3949–3958.
- 829 [70] B. Chankvetadze, Recent development on polysaccharide-based chiral stationary phases for liquid-  
830 phase separation of enantiomers, *J. Chromatogr. A* 1269 (2012) 26-51.
- 831 [71] Y. Okamoto, E. Yashima, Polysaccharide derivatives for chromatographic separation of  
832 enantiomers, *Angew. Chem. Int. Ed.* 37 (1998) 1020-1043.
- 833 [72] Y. Okamoto, M. Kawashima, K. Hatada, XI. Controlled chiral recognition of cellulose  
834 triphenylcarbamate derivatives supported on silica gel, *J. Chromatogr.* 363 (1986) 173-186.
- 835 [73] E. Yashima, E. Kasashima, Y. Okamoto, Enantioseparation on 4-halogen-substituted  
836 phenylcarbamates of amylose as chiral stationary phases for high-performance liquid  
837 chromatography, *Chirality* 9 (1997) 63-68.
- 838 [74] B. Chankvetadze, L. Chankvetadze, S. Sidamonidze, E. Kasashima, E. Yashima, Y. Okamoto, 3-  
839 Fluoro-, 3-chloro- and 3-bromo-5-methylphenylcarbamates of cellulose and amylose as chiral  
840 stationary phases for high-performance liquid chromatographic enantioseparation, *J. Chromatogr.*  
841 *A* 787 (1997) 67-77.

- 842 [75] C. West, M.L. Konjaria, N. Shashviashvili, E. Lemasson, P. Bonnet, R. Kakava, A. Volonterio, B.  
843 Chankvetadze, Enantioseparation of novel chiral sulfoxides on chlorinated polysaccharide  
844 stationary phases in supercritical fluid chromatography, *J. Chromatogr. A* 1499 (2017) 174–182.
- 845 [76] B. Zhu, Y. Yao, M. Deng, Z. Jiang, Q. Li, Enantioselective separation of twelve pairs of  
846 enantiomers on polysaccharide-based chiral stationary phases and thermodynamic analysis of  
847 separation mechanism, *Electrophoresis* 39 (2018) 2398–2405.
- 848 [77] S. Terada, M. Hirai, A. Honzawa, O. Kitagawa, A. Kamizela, A. Wzorek, V.A. Soloshonok,  
849 Possible case of halogen bond-driven self-disproportionation of enantiomers (SDE) via achiral  
850 chromatography, *Chem. Eur. J.* 23 (2017) 14631–14638.
- 851 [78] X. Q. Yan, X. R. Zhao, H. Wang, W. J. Jin, The competition of  $\sigma$ -hole $\cdots$ Cl $^-$  and  $\pi$ -hole $\cdots$ Cl $^-$   
852 bonds between C<sub>6</sub>F<sub>5</sub>X (X = F, Cl, Br, I) and the chloride anion and its potential application in  
853 separation science, *J. Phys. Chem. B* 118 (2014) 1080–1087.

854